An investigation of the effect of phase-randomization of electrons under the influence of an electric field

Hendriks, P.

Award date:
1986

AN INVESTIGATION OF THE EFFECT OF PHASE-RANDOMIZATION OF ELECTRONS UNDER THE INFLUENCE OF AN ELECTRIC FIELD

P.Hendriks

November 1986

NI-86-13

Verslag van een afstudeerwerk in de vakgroep

theoretische natuurkunde

begeleider : Dr. D. Lenstra.

afstudeerhoogleraar : Prof. Dr. W. van Haeringen.

Summary.

The dynamics of non-interacting electrons in a (quasi-) one-dimensional, ringshaped conductor will be treated. The electrons experience both an induced electromotive force and elastic scattering. We will explain how the combination of acceleration and scattering leads to quasi-randomization of the phases, which are present in the time-dependent wave functions. As a consequence of this unexpected and interesting phenomenon one can assign "Ohmic" resistance to the conductor under circumstances where one would not expect it a priori in view of the presence of quantum-interference effects and the absence of a randomizing reservoir.

CONTENTS.

1. INTRODUCTION.

The interest in electronic transport properties of low-dimensional structures has tremendously increased during the past decade. This includes the purely one-dimensional cases although, until present, the interest here has been on a rather theoretical and conceptual level. Nevertheless, the present state of technology has brought us close to or even at the actual fabrication of well-defined nearly one-dimensional systems, such as thin wires and thin rings.

In the present thesis we will report on a theoretical study of electrical conduction in a closed ring-shaped wire, where the cross-section of the wire is thought to be so small that electrons can effectively be treated as one-dimensional.

In a paper by Landauer [1] (nowadays to be considered as a classic paper) a formula is derived which assigns resistance to a one-dimensional system with elastic scattering only, albeit that this formula is claimed, here and in later publications [2], to be applicable under circumstances in which effective phase randomization takes place elsewhere (e.g. in the electrical contacts). Hence, according to Landauer, and later also to Buttiker [3], one-dimensional systems without leads nor any other "source of irreversibility" cannot possibly show resistive behaviour. It is exactly this idea which we will challenge in the present thesis. In fact, we will present evidence that even a model system as simple as a one-dimensional ring in which independent electrons experience elastic scattering due to the presence

of one single delta-function potential, can be assigned resistance although no external phase randomizing mechanism is present at all.

In 1983, Buttiker, Imry and Landauer have dealt with the electrical properties of a normal-metal (i.e. non-superconducting) loop without contacts [4]. They predicted that in response to a constant induced electromotive force, an oscillating current would occur. In view of the clear analogy with the well-known Josephson-oscillations in superconductivity (that is, replace the charge 2e of a Cooper-pair by the charge e of a single electron), the authors introduced the name Josephson-like oscillations.

Two years earlier, Lenstra and van Haeringen [5] developed a dynamic theory of non-interacting electrons in one-dimensional disordered systems driven by an electric field. Since they deal with wave functions which satisfy periodic boundary conditions, their theory is applicable without modification to ring-shaped systems. According to their theory, the system should exhibit normal metallic conduction for not too weak applied electric fields, while for very weak fields one would enter the regime of Bloch-like oscillations, that is, obtain a vanishing DC conductivity. It has also been argued by Lenstra and van Haeringen [6,7] that the current response can be described, at least qualitatively, with the use of a Boltzmann-type of equation. However, the aspect of randomization remained obscure, until recently two articles appeared in which self-randomization is shown to occur as a consequence of the electron dynamics, even though no external randomizing mechanism is present [8,9].

The purpose of the present thesis is to explicitly work out the above-mentioned ideas for about the simplest model system one can possibly think of in the theory of electronic conduction. The system to be studied is a ring in which the electrons can be treated as non-interacting and free to move in one dimension only. These electrons experience scattering due to one single delta-function potential.

The theory is developed in chapter 2. The stationary states and energy spectrum for the ring with delta-function potential are obtained in section 2.3. Time dependence is introduced in section 2.4 where we derive equations which govern the time-evolution of probability amplitudes under the influence of a driving electric field. How the dynamics give rise to reversibility on the one hand and phase randomization on the other hand, is shown in section 2.5.

Chapter 3 is fully devoted to a presentation of numerical results obtained with the algorithm based on the theory of chapter 2. Charge distributions, electrical current and energies are being calculated. A new quantity is introduced and calculated. This quantity is shown to behave in some respects as an entropy, which it is not.

The important question as to whether the results of chapter 3 also could have been derived, at least qualitatively, with the use of a Boltzmann-type of equation is dealt with in chapter 4. A Boltzmann equation is derived (section 4.1), and integrated in order to obtain the solution, with the use of which current, energy and entropy are calculated (section 4.2) and confronted with the results of chapter 3 (section 4.3).

2. QUANTUM-MECHANICAL THEORY OF A CLOSED ONE-DIMENSIONAL LOOP.

2.1 .Basic theory.

In this section we will develop the general theory of the dynamics of non-interacting electrons in a one-dimensional (1D) loop. The system, which we consider, consists of a normal-metal (i.e. non-superconducting) ring with circumference L and a potential U(x), where x measures the position along the wire (see figure 2.1.1.). We assume, that the cross-section of the wire is sufficiently small, justifying a one-dimensional treatment. We will treat the electrons as non-interacting fermions, which, as a matter of course, satisfy the Pauli-principle. All relevant quantities, which we will calculate lateron, such as the charge-density distribution, the electrical current and the total energy, are additive in the contributions due to each

Fig. 2.1.1. The (quasi-) one-dimensional loop, encompassing a magnetic field. By varying the magnetic field in time, an electromotive force is induced in the loop.

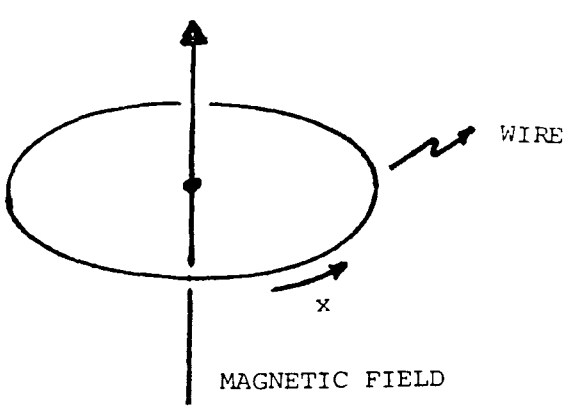

independently moving electron. In order to study the dynamics of the electrons, we assume the presence of an induced electromotive force, which is due to a time-dependent magnetic flux, encompassed by the loop. If A is the component of the vectorpotential along the loop, associated with the applied magnetic field, then the wave function of one electron in the ring is a solution of the time-dependent Schrödinger equation

$$i\hbar \frac{\partial \Psi(x,t)}{\partial t} = \left(\frac{1}{2m} \{ \frac{\hbar}{i} \frac{\partial}{\partial x} - eA \}^2 + U(x) \right) \Psi(x,t) \ , \qquad (2.1.1)$$

subject to the periodic boundary conditions

$$\Psi(x+L,t) = \Psi(x,t) \ . \qquad (2.1.2)$$

In principle, knowledge of all one-electron wave functions at all times t allows us to calculate the above-mentioned quantities. To be specific, the charge-density $\rho(x,t)$, the current $j(t)$ and the energy $E(t)$ are given by

$$\rho(x,t) = e|\Psi(x,t)|^2 \qquad (2.1.3)$$

$$j(t) = \frac{e}{m} \int_0^L dx \ \Psi(x,t)^* \left[\frac{\hbar}{i} \frac{\partial}{\partial x} - eA \right] \Psi(x,t) \qquad (2.1.4)$$

and

$$E(t) = \int_0^L dx \ \Psi(x,t)^* \left[\frac{1}{2m} \left[\frac{h}{i} \frac{\partial}{\partial x} - eA \right]^2 + U(x) \right] \Psi(x,t) \qquad (2.1.5)$$

Since we intend to study the action of a constant electric field along the loop, we will assume that A depends linearly on time, i.e.

$$A = -Ft \ , \qquad (2.1.6)$$

where the constant F is the magnitude of the electric field.

To solve the Schrödinger equation (2.1.1) we will use the expansion

$$\Psi(x,t) = \sum_l c_l(t)\, u_l^{\alpha(t)}(x) \ , \tag{2.1.7}$$

where

$$\alpha(t) = eFLt/\hbar \ , \tag{2.1.8}$$

while the functions $u_l^{\alpha}(x)$ satisfy the time-independent or "stationary" Schrödinger equation

$$\left[\frac{\hbar^2}{2m} \left(\frac{1}{i} \frac{\partial}{\partial x} + \frac{\alpha}{L} \right)^2 + U(x) \right] u_l^{\alpha}(x) = \epsilon_l^{\alpha}\, u_l^{\alpha}(x) \tag{2.1.9}$$

with boundary condition

$$u_l^{\alpha}(x+L) = u_l^{\alpha}(x) \tag{2.1.10}$$

The advantage of representation (2.1.7) is that $\Psi(x,t)$ is expressed as a time-dependent linear combination of the "stationary" states $u_l^{\alpha}(x)$ with eigenenergies ϵ_l^{α}. The time t, however, is present in these "stationary" states, but only as a parameter via α as given in (2.1.8). Transitions of one "stationary" state to another will manifest themselves by the time-dependence of the absolute values of the coefficients $c_l(t)$.

The functions $\varphi_l^{\alpha}(t)$, which are related to the $u_l^{\alpha}(t)$'s by

$$\varphi_l^{\alpha}(t) = e^{i\alpha x/L}\, u_l^{\alpha}(t) \ , \tag{2.1.11}$$

satisfy the usual Schrödinger equation

$$\left[-\frac{\hbar^2}{2m} \frac{\partial^2}{\partial x^2} + U(x) \right] \varphi_l^{\alpha}(x) = \epsilon_l^{\alpha}\, \varphi_l^{\alpha}(x) \ , \tag{2.1.12}$$

with the rather unusual boundary condition

$$\varphi_l^{\alpha}(x+L) = e^{i\alpha}\, \varphi_l^{\alpha}(x). \tag{2.1.13}$$

In the next sections we will solve (2.1.12) for some special potentials U(x). Note that solving (2.1.12) subject to (2.1.13) is fully equivalent to solving (2.1.9) subject to (2.1.10). For later convenience and following Lenstra and van Haeringen [5], we will choose an eventual α-dependence in the $u_l^\alpha(x)$ such that

$$\int_0^L dx\, u_l^\alpha(x)^* \frac{\partial}{\partial\alpha} u_l^\alpha(x) = 0 \ . \tag{2.1.14}$$

For later use we also mention the relation (for $l \neq l'$)

$$\int_0^L dx\, u_l^\alpha(x)^* \frac{\partial}{\partial\alpha} u_{l'}^\alpha(x) = \frac{i\hbar^2/mL}{\epsilon_l^\alpha - \epsilon_{l'}^\alpha} \int_0^L dx\, u_l^\alpha(x)^* \frac{\partial}{\partial x} u_{l'}^\alpha(x) \ , \tag{2.1.15}$$

the complete proof of which can be found in [10].

Next we sustitute (2.1.7) in (2.1.1) and multiply the obtained expression with $u_k^{\alpha(t)}(x)^*$, where the asterix * denotes the complex conjungate. After integration over x from 0 to L we obtain the following set of differential equations for the $c_k(t)$'s :

$$\frac{d}{dt}c_k(t) = \left(\frac{-i}{\hbar} \epsilon_k^\alpha c_k(t) - \sum_{l\neq k} \left[\frac{ieF\hbar/m}{\epsilon_k^\alpha - \epsilon_l^\alpha} \int_0^L dx \{ \varphi_k^\alpha(x)^* \frac{\partial}{\partial x} \varphi_l^\alpha(x) \} \right] c_l(t) \right) \Bigg|_{\alpha=\alpha(t)} , \tag{2.1.16}$$

where we used (2.1.15).

The original problem of determining the solution of (2.1.1) has been reformulated in terms of solving either (2.1.9) or (2.1.12) in order to obtain "stationary" states, and solving (2.1.16) in order to obtain the respective probability amplitudes.

The expressions for the charge density $\rho(x,t)$, the electrical current $j(t)$ and the energy $E(t)$, in terms of the $\varphi_l^{\alpha(t)}(x)$'s and the $c_l(t)$'s, are given by (see (2.1.3) to (2.1.5))

$$\rho(x,t) = e \left|\sum_{l} c_l(t)\, \varphi_l^{\alpha(t)}(x)\right|^2, \tag{2.1.17}$$

$$j(t) = \frac{-ie\hbar}{m} \sum_{l,l'} \left[\int_o^L dx\, \varphi_l^{\alpha(t)}(x)^* \frac{\partial}{\partial x} \varphi_{l'}^{\alpha(t)}(x) \right] c_l(t)^* c_{l'}(t) \tag{2.1.18}$$

and

$$E(t) = \sum_{l,l'} \left[\int_o^L dx \{\varphi_l^{\alpha(t)}(x)^* \left[\frac{-\hbar^2}{2m} \frac{\partial^2}{\partial x^2} + U(x)\right] \varphi_{l'}^{\alpha(t)}(x)\} c_l(t)^* c_{l'}(t) \right] \tag{2.1.19}$$

where it is understood that the $\varphi_l^{\alpha(t)}(x)$-functions are normalized to unity.

We want to emphasize, that (2.1.17), (2.1.18) and (2.1.19) are expressions for one electron. To obtain results for more electrons we have to add the contributions due to each electron. In general, each contribution will be different due to the fact that the electrons initially occupy different states (the Pauli-principle). Furthermore, if we start with orthonormal wave functions, they remain orthonormal, since the time-evolution operator is unitary. This implies that if the Pauli-principle initially holds, it will allways hold. In the next three sections, we will derive expressions for the $\varphi_l^{\alpha(t)}(x)$'s and the $c_l(t)$'s in the empty-lattice case (U(x) = 0) and in the case of a delta-function potential.

2.2. Application to the empty-lattice case.

Here we will assume that the potential U(x) equals zero everywhere. The solutions of the time-independent Schrödinger equation (2.1.12) with boundary condition (2.1.13) are then given by

$$\tilde{\varphi}_l^{\alpha}(x) = \frac{1}{\sqrt{L}} e^{i(2\pi l+\alpha)x/L}, \qquad (2.2.1)$$

with $l = 0, \pm 1, \pm 2, \ldots$ (we will use a tilde ~ to indicate quantities corresponding to the empty-lattice case). As a consequence the u-functions (see (2.1.11)) in this case are given by

$$\tilde{u}_l^{\alpha}(x) = \frac{1}{\sqrt{L}} e^{i(2\pi l)x/L}. \qquad (2.2.2)$$

Note that both $\tilde{\varphi}_l^{\alpha}(x)$ and $\tilde{u}_l^{\alpha}(x)$ fulfil the orthonormality condition

$$\int_0^L dx\ \tilde{\varphi}_l^{\alpha}(x)^* \tilde{\varphi}_{l'}^{\alpha}(x) = \int_0^L dx\ \tilde{u}_l^{\alpha}(x)^* \tilde{u}_{l'}^{\alpha}(x) = \delta_{ll'}. \qquad (2.2.3)$$

The corresponding eigenenergies are given by the parabolic functions

$$\tilde{\epsilon}_l^{\alpha} = \frac{\hbar^2}{2mL^2}(2\pi l+\alpha)^2 \qquad (2.2.4)$$

After substitution of (2.2.1) in (2.1.16) it can be seen that the second term on the right-hand side of (2.1.16) will vanish. Hence (2.1.16) reduces to a simple set of independent first order differential equations with solutions

$$c_l(t) = c_l(0)\ \exp\Big[\int_0^t dt' \{\frac{-i}{\hbar}\tilde{\epsilon}_l^{\alpha}(t')\}\Big] \qquad (2.2.5)$$

In fig 2.2.1 the energy spectrum (2.2.4) is shown. If we start with $c_l(0) = \delta_{ll'}$ (i.e. the initial values belonging to an eigenstate), it is impossible that a coefficient $c_{l'}(t)$ with $l \neq l'$ will become non-zero,

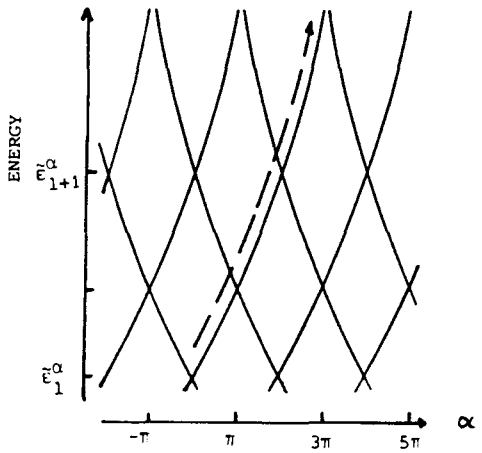

Fig.2.2.1. Energy spectrum in the empty-lattice case. The arrow indicates the trajectory in (E-α)space of an electron under the influence of a constant electric field.

since the equations for the $c_l(t)$'s are not coupled (see (2.2.5)). This implies that an electron will stay in the same band if time goes by, which is illustrated by the arrow in fig. 2.2.1. In this case the current is linearly increasing with time (see (2.1.18)), while the energy is quadratic in time (see (2.2.4)).

In fig 2.2.1 one also notices that degeneracies occur at the intersections of parabolic bands, i.e. at $\alpha = q\pi$, with $q = 0, \pm1, \pm2, \ldots$ One of the main effects of a weak non-zero potential is to remove these degeneracies (see fig. 2.2.2); another implication is that the equation for the $c_l(t)$'s (2.1.16) will be coupled. If we start again with an eigenstate labeled by l, the $c_{l'}(t)$'s with $l' \neq l$ will now become non-zero in the course of time. Note that both in the empty-lattice case and in the case of a non-zero potential the eigenenergy spectrum is periodic in α with period 2π.

Fig.2.2.2. Energy spectrum in the case of a weak potential. One notices that the degeneracies which were present in the empty-lattice-case disappeared, while the structure is still periodic in α with period 2π.

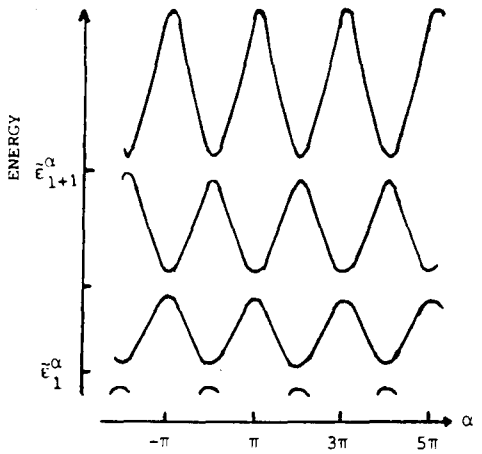

In order to study a well-defined system with elastic scattering, we will consider in the next section a potential of the form $C*\delta(x)$, where C is a sufficiently small constant.

2.3. "Stationary" states and energy spectrum for a weak delta-function potential.

In this section we will assume that the potential U(x) is given by

$$U(x) = pL\ \delta(x), \qquad (2.3.1)$$

where p is a measure for the strength of the potential. We assume that p>0 and sufficiently small, as will be specified lateron.

Since the set of functions (2.2.1), i.e. the set $\{\frac{1}{\sqrt{L}} e^{i(2\pi l+\alpha)x/L}\}$, with l = 0, ±1, ±2,..., is a complete set compatible with the boundary condition (2.1.13), we can expand the eigenfunctions $\varphi_l^{\alpha}(t)$ of (2.1.12) in these plane waves. We assume that the potential is sufficiently weak, so that solutions for the "stationary" wave functions and the energy spectrum can be obtained by using degenerate perturbation theory near each band-intersection. In practice, this means that we approximate the perturbed wave functions in the neighbourhood of a degeneracy by a linear combination of the two unperturbed plane waves which were to be degenerate in the empty-lattice case. Within one period of α (i.e. $-\pi/2<\alpha<3\pi/2$) two types of degeneracies show up; those which occur at $\alpha=0$ (type I) and those which occur at $\alpha=\pi$ (type II). This is also illustrated in fig 2.3.2. The unperturbed wave functions to be considered in the neighbourhood of $\alpha=0$ are (without the normalization factor) $e^{i(2\pi l+\alpha)+i\chi_1(\alpha)}$ and $e^{-i(2\pi l-\alpha)+i\chi_2(a)}$, while the corresponding eigenenergies are given by $\tilde{\epsilon}_{\pm l}^{\alpha} = \frac{\hbar^2}{2mL^2}(2\pi l+\alpha)^2$. We have added α-dependent phase factors $\exp[i\chi_1(\alpha)]$ and $\exp[i\chi_2(\alpha)]$ to the unperturbed plane waves. The functions $\chi_1(\alpha)$ and $\chi_2(\alpha)$ will be specified lateron to ensure

the continuity of the wave functions and their derivatives with respect to α. In the presence of the delta-function potential, the (perturbed) wave functions $\varphi_l^\alpha(x)$ will be written as

$$\varphi_l^\alpha(x) = \frac{1}{\sqrt{L}} \left[a e^{i(2\pi l+\alpha)x/L + i\chi_1(\alpha)} + b e^{i(-2\pi l+\alpha)x/L + i\chi_2(\alpha)} \right] \quad (2.3.2)$$

Using standard methods, we arrive at the set of equations for a and b

$$\begin{pmatrix} \tilde{\epsilon}_l^\alpha - \epsilon^\alpha + p & p\, e^{i(\chi_2(\alpha)-\chi_1(\alpha))} \\ p\, e^{i(\chi_1(\alpha)-\chi_2(\alpha))} & \tilde{\epsilon}_{-l}^\alpha - \epsilon^\alpha + p \end{pmatrix} \begin{pmatrix} a \\ b \end{pmatrix} = \begin{pmatrix} 0 \\ 0 \end{pmatrix} \quad (2.3.3)$$

This set has non-trivial solutions only when the determinant vanishes. Equating the latter to zero then yields for the eigenenergies

$$\epsilon_{l,\pm}^\alpha = \frac{1}{2} \{ \tilde{\epsilon}_l^\alpha + \tilde{\epsilon}_{-l}^\alpha + 2p \pm \sqrt{(\tilde{\epsilon}_l^\alpha - \tilde{\epsilon}_{-l}^\alpha)^2 + 4p^2} \} \quad (2.3.4)$$

For these eigenenergies the coefficients a and b satisfy

$$b = h_{l\alpha}\, a \qquad \text{(in the case of } \epsilon_{l,+}) \quad (2.3.5)$$

and

$$a = -h_{l\alpha}^*\, b \quad \text{(in the case of } \epsilon_{l,-}), \quad (2.3.6)$$

where

$$h_{l\alpha} = \left[\left\{ \left(\frac{\tilde{\epsilon}_l^\alpha - \tilde{\epsilon}_{-l}^\alpha}{2p} \right)^2 + 1 \right\}^{1/2} - \left(\frac{\tilde{\epsilon}_l^\alpha - \tilde{\epsilon}_{-l}^\alpha}{2p} \right) \right] e^{-i(\chi_2(a)-\chi_1(\alpha))} \quad (2.3.7)$$

The normalized wave functions can now be expressed as

$$\varphi_{l,+}^\alpha = \frac{(1+|h_{l\alpha}|^2)^{-1/2}}{\sqrt{L}} \left[e^{i(2\pi l+\alpha)x/L + i\chi_1(\alpha)} + h_{l\alpha} e^{i(-2\pi l+\alpha)x/L + i\chi_2(\alpha)} \right] \quad (2.3.8)$$

and

$$\varphi_{l,-}^\alpha = \frac{(1+|h_{l\alpha}|^2)^{-1/2}}{\sqrt{L}} \left[h_{l\alpha}^* e^{i(2\pi l+\alpha)x/L + i\chi_1(\alpha)} - e^{i(-2\pi l+\alpha)x/L + i\chi_2(\alpha)} \right] \quad (2.3.9)$$

Equations (2.3.8) and (2.3.9) refer to values of α such that $-\pi/2 < \alpha < \pi/2$

Fig.2.3.1. Bandlabeling to be used throughout this report.

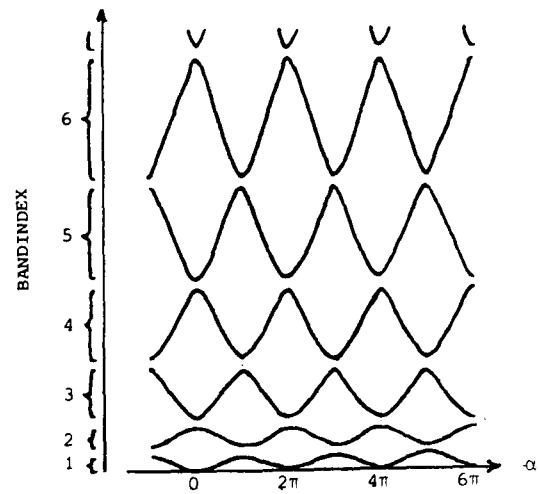

(type I degeneracies). The situation for $\pi/2<\alpha<3\pi/2$ is completely equivalent, but more complicated due to the asymmetry in the labeling of the plane waves involved. Thusfar, the perturbed wave functions have been labeled using the l-index, which belongs to the composing plane waves. It will be more convenient to use a new labeling, such that each periodic (as a function of α) energy band is labeled by one and the same index. We will therefore label the bands by n = 1,2,3,... starting from the lowest band (see fig 2.3.1). The wave functions corresponding to the n-th band will be denoted by $\phi_n^\alpha(x)$ (see fig 2.3.2), where it is understood that $\phi_n^\alpha(x)$, $\partial\phi_n^\alpha(x)/\partial x$ and $\partial\phi_n^\alpha(x)/\partial\alpha$ are continuous function of both x and α.

It is clear that $\phi_n^\alpha(x)$ is given by different $\varphi_l^\alpha(x)$-functions, depending on whether α mod (2π) (i.e. α reduced to the interval $[-\pi/2,3\pi/2]$) corresponds to a type I or a type II degeneracy. For the

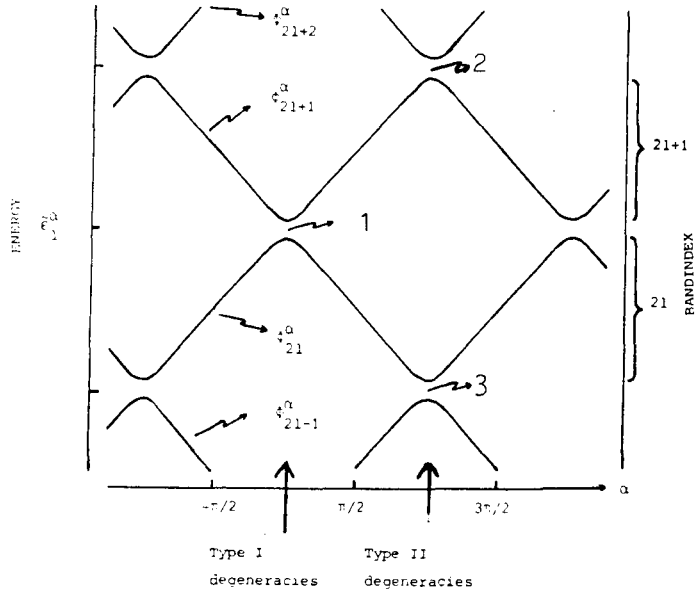

Fig.2.3.2. Detail of the energy spectrum in the case of a delta-function potential. The two different types of degeneracies are indicated. The ϕ^{α}_{n}*'s are the wavefunctions belonging to band n.*

type I situation with $-\pi/2<\alpha<\pi/2$ we will identify

$$\phi^{\alpha}_{2l+1}(x) = \varphi^{\alpha}_{l,+}(x) \quad \text{(odd-numbered bands)} \tag{2.3.11}$$

and

$$\phi^{\alpha}_{2l}(x) = \varphi^{\alpha}_{l,-}(x) \quad \text{(even-numbered bands)} \tag{2.3.12}$$

with $\varphi^{\alpha}_{l,+}(x)$ and $\varphi^{\alpha}_{l,-}(x)$ as given in (2.3.8) and (2.3.9). For the type II degeneracies we will apply the same method. Since we want to determine the wave functions $\phi^{\alpha}_{2l}(x)$ and $\phi^{\alpha}_{2l+1}(x)$, we have to use perturbation theory near the degeneracies 2 and 3, respectively (see fig 2.3.2). The result are ($\pi/2<\alpha<3\pi/2$)

$$\phi^{\alpha}_{2l+1}(x)=\frac{(1+|h_{2\alpha}|^2)^{-1/2}}{\sqrt{L}}\left[h^{*}_{2\alpha}e^{i(2\pi l+\alpha)x/L+i\chi_3(\alpha)}-e^{i(-2\pi(l+1)+\alpha)x/L+i\chi_4(\alpha)}\right] \tag{2.3.12}$$

and

$$\phi^{\alpha}_{21}(x)=\frac{(1+|h_{3\alpha}|^2)^{-1/2}}{\sqrt{L}}\left[e^{i(2\pi(l-1)+\alpha)x/L+i\chi_5(\alpha)}+h_{3\alpha}e^{i(-2\pi l+\alpha)x/L+i\chi_6(\alpha)}\right], \tag{2.3.13}$$

where

$$h_{2\alpha}=\left[\left\{\left(\frac{\tilde{\epsilon}^{\alpha}_{l}-\epsilon^{\alpha}_{-l-1}}{2p}\right)^2+1\right\}^{1/2}-\left(\frac{\tilde{\epsilon}^{\alpha}_{l}-\tilde{\epsilon}^{\alpha}_{-l-1}}{2p}\right)\right]e^{i(\chi_3(\alpha)-\chi_4(\alpha))} \tag{2.3.14}$$

and

$$h_{3\alpha}=\left[\left\{\left(\frac{\tilde{\epsilon}^{\alpha}_{l-1}-\tilde{\epsilon}^{\alpha}_{-l}}{2p}\right)^2+1\right\}^{1/2}-\left(\frac{\tilde{\epsilon}^{\alpha}_{l-1}-\tilde{\epsilon}^{\alpha}_{-l}}{2p}\right)\right]e^{i(\chi_5(\alpha)-\chi_6(\alpha))} \tag{2.3.15}$$

In (2.3.12) and (2.3.13) the phase angles χ_3, χ_4, χ_5 and χ_6 serve the same pupose as χ_1 and χ_2 before did; their presense enables us to make "smooth" connections between the different representations of $\phi^{\alpha}_{21}(x)$ and $\phi^{\alpha}_{2l+1}(x)$ as function of α.

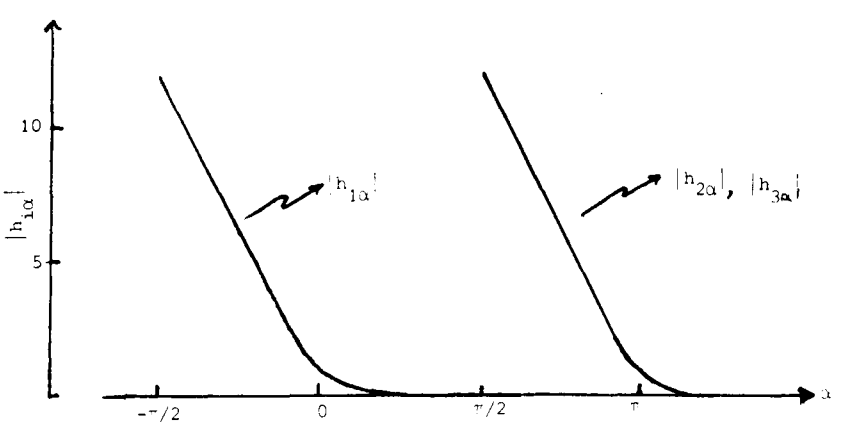

Fig.2.3.3. Illustrating the qualitative behaviour of the $|h_{1\alpha}|$, $|h_{2\alpha}|$ *and* $|h_{3\alpha}|$ *as a function of* α.

As announced, we assume p to be small. To be precise, we assume that p is much smaller than the average distance between two energy bands near the Fermi-energy. This implies that $|h_{1\alpha}|>>1$ for $\alpha=-\pi/2$ and $|h_{1a}|$ is almost zero for $\alpha=\pi/2$. For $|h_{2\alpha}|$ and $|h_{3\alpha}|$, relations of the same kind hold at $\alpha=\pi/2$ and $\alpha=3\pi/2$. Examples of $|h_{1\alpha}|$, $|h_{2\alpha}|$ and $|h_{3\alpha}|$ as function of α can be seen in fig.2.3.3.The behaviour of $h_{1\alpha}$, $h_{2\alpha}$ and $h_{3\alpha}$, as observed in (2.3.8), (2.3.9), (2.3.12) and (2.3.13) implies that we may represent in good approximation the $\phi_n^\alpha(x)$'s by single plane waves at $\alpha=-\pi/2$, $\pi/2$ and $3\pi/2$.

We now have expressions for the $\phi_n^\alpha(x)$'s for $-\pi/2<\alpha<3\pi/2$. For values of α outside this interval we can simply reduce α to the interval $[-\pi/2,3\pi/2]$ by use of the modulo operation. The procedure leads to different expressions for different α-regions, i.e. after reduction to the α-interval $[-\pi/2,\pi/2]$ and $[\pi/2,3\pi/2]$. However, we must ensure the continuity of $\phi_n^\alpha(x)$ and $\partial\phi_n^\alpha(x)/\partial\alpha$ as functions of α. This can be done by proper choices of the phase angles $\chi_m(\alpha)$. Choosing $\chi_1=\chi_3=\chi_5=0$, $\chi_2=\alpha+\pi/2$, and $\chi_4=\chi_6=\alpha-\pi/2$ will make $\phi_n^\alpha(x)$ and $\partial\phi_n^\alpha(x)/\partial\alpha$ continous functions of α. The stationary wave functions are now given by

$$\phi_{2l+1}^\alpha(x) = \frac{(1+|h_{1\alpha}|^2)^{-1/2}}{\sqrt{L}} \left[e^{i(2\pi l+\alpha)x/L} + h_{1\alpha} e^{i((-2\pi l+\alpha)x/L+\alpha+\pi/2))} \right] \tag{2.3.16}$$

and

$$\phi_{2l}^\alpha = \frac{(1+|h_{1\alpha}|^2)^{-1/2}}{\sqrt{L}} \left[h_{1\alpha}^* e^{i(2\pi l+\alpha)x/L} - e^{i(-2\pi l+\alpha)x/L+\alpha+\pi/2)} \right] \tag{2.3.17}$$

for the α-interval $[-\pi/2,\pi/2]$, while

$$\phi^{\alpha}_{2l+1}(x)=\frac{(1+|h_{2\alpha}|^2)^{-1/2}}{\sqrt{L}}\left[h^{*}_{2\alpha}e^{i(2\pi l+\alpha)x/L}-e^{i((-2\pi(l+1)+\alpha)x/L+\alpha-\pi/2)}\right] \tag{2.3.18}$$

and

$$\phi^{\alpha}_{2l}(x)=\frac{(1+|h_{3\alpha}|^2)^{-1/2}}{\sqrt{L}}\left[e^{i(2\pi(l-1)+\alpha)x/L}+h_{3\alpha}e^{i((-2\pi l+\alpha)x/L+\alpha-\pi/2))}\right], \tag{2.3.19}$$

for α in the interval $[\pi/2,3\pi/2]$.

Note that in this form the ϕ^{α}_{n}-functions are not only smoothly connected at $\alpha=\pi/2$ but also at $\alpha=3\pi/2$ and so on.

The small discontinuities, which still exist at α mod (π) = $\pi/2$ are related to the fact that the $h_{i\alpha}$-functions (see fig 2.3.3) are not zero or infinite at $\alpha=-\pi/2$, $\pi/2$ and $3\pi/2$. This is the price paid for the simple two-wave mixing model employed here. However we do not think that this will affect any of the conclusions to be drawn lateron.

2.4. Time-dependent probability amplitudes in the presence of a delta-function potential.

In section 2.1 we have derived a set of differential equations for the $c_n(t)$'s (see (2.1.16)). We will now substitute the expressions (2.3.16) to (2.3.19) for the $\varphi_n^{\alpha(t)}(x)$'s in (2.1.16). We then notice that -within α-intervals $[(q-1/2)\pi,(q+1/2)\pi]$ with $q = 0, \pm1, \pm2,...$- the coupling of the differential equations almost vanishes except for the coupling between the two neighbouring bands, which resulted from the degeneracy removal. Hence, for each respective α-interval of length π, the set of differential equations (2.1.16) splits in subsets of only two equations, which can be solved independently. For $-\pi/2<\alpha<\pi/2$ the coefficients $c_{2l}(t)$ and $c_{2l+1}(t)$ are coupled, while for $\pi/2<\alpha<3\pi/2$, $c_{2l-1}(t)$ and $c_{2l}(t)$ are coupled with $l = 1, 2, 3,...$. As a representative example for all other subsets we will solve the two equations belonging to bands 2l+1 and 2l, with $-\pi/2<\alpha<\pi/2$. The equations are given by

$$\frac{d}{dt}c_{2l+1}(t) = \left[\frac{i}{\hbar}\epsilon^{\alpha}_{2l+1}c_{2l+1}(t) - \frac{ieF\hbar/m}{E^{\alpha}_{2l+1,2l}} D^{\alpha}_{2l+1,2l}\, c_{2l}(t)\right]\Bigg|_{\alpha=\alpha(t)}$$

$$\frac{d}{dt}c_{2l}(t) = \left[\frac{i}{\hbar}\epsilon^{\alpha}_{2l}\, c_{2l}(t) - \frac{ieF\hbar/m}{E^{\alpha}_{2l+1,2l}} D^{\alpha *}_{2l+1,2l}\, c_{2l+1}(t)\right]\Bigg|_{\alpha=\alpha(t)} \qquad (2.4.1)$$

where

$$E^{\alpha}_{2l+1,2l} = \epsilon^{\alpha}_{2l+1,2l} - \epsilon^{\alpha}_{2l} = \left[(\tilde{\epsilon}^{\alpha}_{l} - \tilde{\epsilon}^{\alpha}_{-l})^2 + 4p^2\right]^{1/2}, \qquad (2.4.2)$$

$$D^{\alpha}_{2l+1,2l} = \int_0^L dx\, \Phi^{\alpha}_{2l+1}(x)^* \frac{\partial}{\partial x} \Phi^{\alpha}_{2l}(x) = \frac{h_{l\alpha}}{1+|h_{l\alpha}|^2}\, 4\pi i l/L, \qquad (2.4.3)$$

and ϵ^{α}_n denotes the energy of band n.

Introducing the abbreviations

$$n = 2l; \qquad z_n = \frac{\hbar^2 n\pi^2}{2mL^2p}; \qquad \gamma_n = \frac{2p^2mL}{eF\hbar^2 n\pi}; \qquad z = \frac{\hbar n\pi eFt}{Lmp}, \tag{2.4.4}$$

we can write (2.4.1) in the more convenient form

$$\begin{aligned} \frac{d}{dz}c_{n+1}(z) &= -i\gamma_n\left(z_n\frac{n}{2} + \frac{z^2}{8z_n n} + \frac{1}{2} + \frac{1}{2}\sqrt{z^2+1}\right) c_{n+1}(z) + \\ &\quad \frac{1}{2(z^2+1)}\, c_n(z) \\ \frac{d}{dz}c_n(z) &= -i\gamma_n\left(z_n\frac{n}{2} + \frac{z^2}{8z_n n} + \frac{1}{2} - \frac{1}{2}\sqrt{z^2+1}\right) c_n(z) + \\ &\quad \frac{-1}{2(z^2+1)}\, c_{n+1}(z) \end{aligned} \tag{2.4.5}$$

and these equations should be solved for $-z_n < z < z_n$, which is equivalent to $-\pi/2 < \alpha < \pi/2$. We prefer, instead of dealing with (2.4.5), to introduce the transformation

$$\begin{aligned} b_{n+1}(z) &= c_{n+1}(z)\, \exp\left[i\gamma_n \int_o^z dy\left(z_n\frac{n}{2} + \frac{y^2}{8z_n n} + \frac{1}{2} + \frac{1}{2}\sqrt{y^2+1}\right)\right] \\ b_n(z) &= c_n(z)\, \exp\left[i\gamma_n \int_o^z dy\left(z_n\frac{n}{2} + \frac{y^2}{8z_n n} + \frac{1}{2} - \frac{1}{2}\sqrt{y^2+1}\right)\right], \end{aligned} \tag{2.4.6}$$

after which (2.4.5) transforms into

$$\begin{aligned} \frac{d}{dz}b_{n+1}(z) &= \frac{1}{2(z^2+1)}\, \exp\left[i\gamma_n \int_o^z dy\, \sqrt{y^2+1}\,\right] b_n(z) \\ \frac{d}{dz}b_n(z) &= \frac{-1}{2(z^2+1)}\, \exp\left[-i\gamma_n \int_o^z dy\, \sqrt{y^2+1}\,\right] b_{n+1}(z) \end{aligned} \tag{2.4.7}$$

In the actual numerical procedure, we will deal with (2.4.7). Once the initial values of $b_{n+1}(z)$ and $b_n(z)$ at $z = -z_n$ are given, the values of $b_{n+1}(z)$ and $b_n(z)$ can be calculated by integration of (2.4.7) from $-z_n$ to z_n and the results can be summarized by the matrix multiplication

$$\begin{pmatrix} b_{n+1}(z_n) \\ b_n(z_n) \end{pmatrix} = \begin{pmatrix} R_n & T_n \\ -T_n^* & R_n^* \end{pmatrix} \begin{pmatrix} b_{n+1}(-z_n) \\ b_n(-z_n) \end{pmatrix}, \qquad (2.4.8)$$

where R_n and T_n are scalar quantities.

One easily proofs that the transition matrix (2.4.8) is unitary, which implies that $|T_n|^2 + |R_n|^2 = 1$. Since numerical results show, that T_n is real and positive, we only have to calculate R_n as a function of z_n and γ_n. The results are shown in fig 2.4.1^a and 2.4.1^b, for $100 \leq z_n \leq 1000$ and $10^{-4} \leq \gamma_n \leq 10^{-1}$. The numerical results show that for γ_n not too small ($\gamma_n > \gamma_{min}$, where γ_{min} is a decreasing function of increasing z_n) we have in good approximation $|R_n| \rightarrow \exp(-\pi\gamma_n/4)$. The argument of R_n may be approximated by $-\pi/4$, at least in a certain region of the (z_n, γ_n)-plane (see fig 2.4.1^b).

Having obtained solutions for the $b_n(z_n)$'s, we can now use the inverse of (2.4.6) to obtain solutions for the $c_n(z_n)$'s. This yields

$$\begin{pmatrix} c_{n+1}(z_n) \\ c_n(z_n) \end{pmatrix} = e^{-iA_n} \begin{pmatrix} e^{-iB_n} R_n & T_n \\ -T_n^* & e^{iB_n} R_n^* \end{pmatrix} \begin{pmatrix} c_{n+1}(-z_n) \\ c_n(-z_n) \end{pmatrix}, \qquad (2.4.9)$$

where

$$A_n = z_n^2 \gamma_n (n + \frac{1}{12n}) + z_n \gamma_n \qquad (2.4.10)$$

$$B_n = \frac{1}{2} z_n \gamma_n \sqrt{1+z_n^2} + \frac{\gamma_n}{2} \ln(z_n + \sqrt{1+z_n^2}). \qquad (2.4.11)$$

If we perform these matrix multiplications for all two by two subsets in the interval $-z_n < z < z_n$ we are able to calculate all $c_n(z_n)$'s. Since for other α-intervals the procedure is completely equivalent, it is now possible to determine the $c_n(t)$'s at $\alpha=(q-1/2)\pi$, with $q=1,2,3,\ldots$, if their values at, say, $\alpha = -\pi/2$ are known. The whole problem has been reduced to succesive matrix multiplications, where each

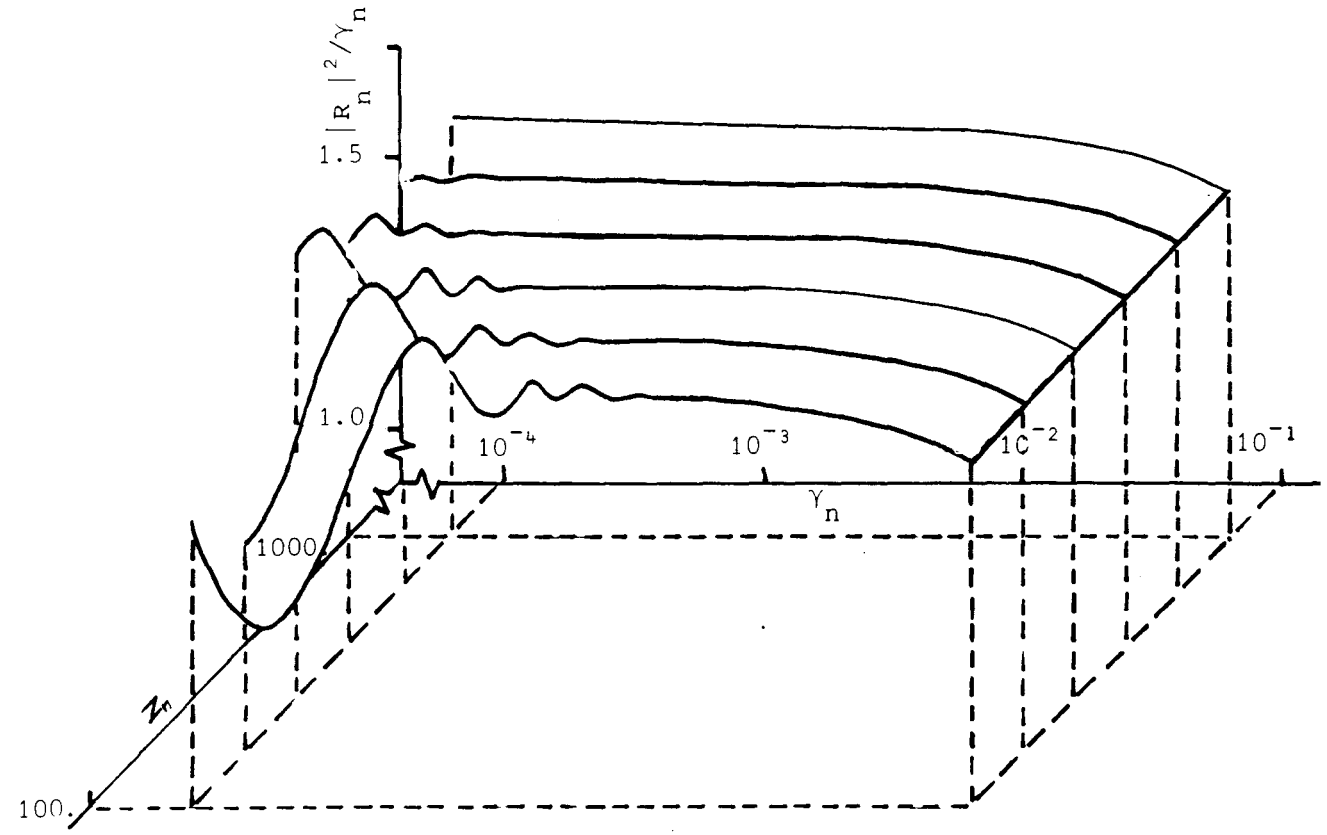

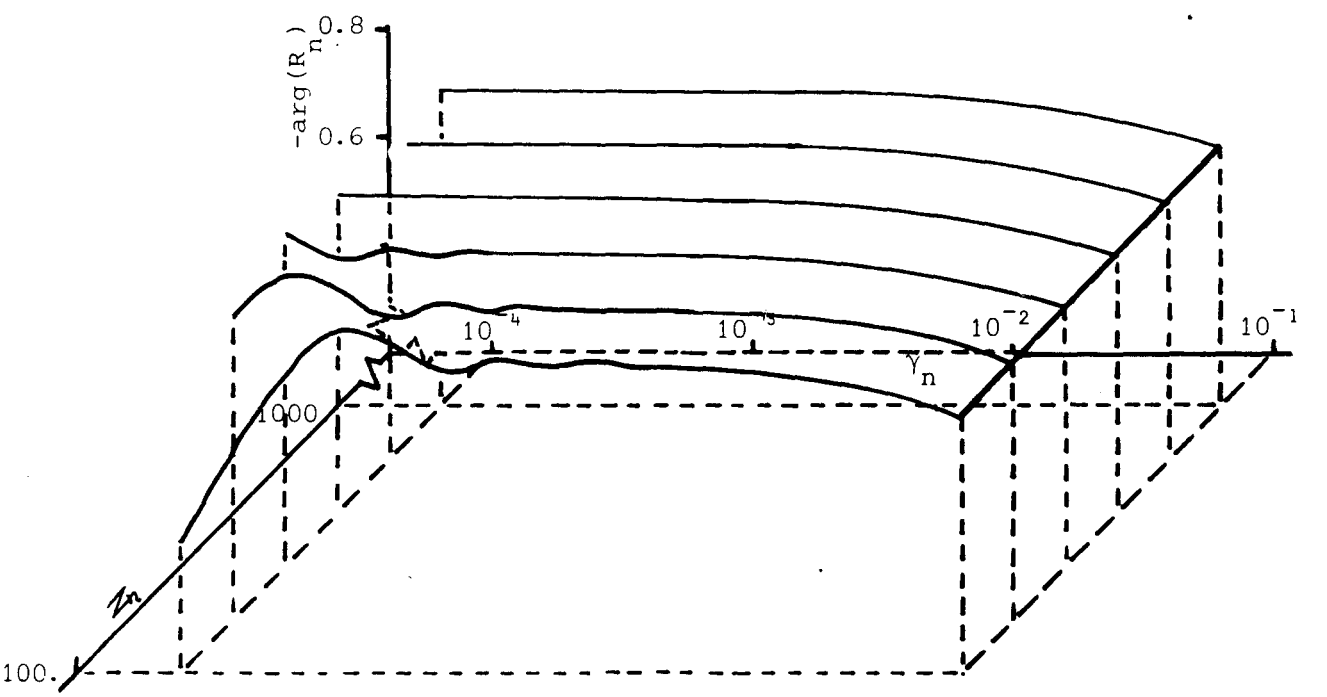

Fig.2.4.1[a,b] *The absolute value and argument of* R_n. *In fig 2.4.1.*[a] $|R_n|^2/\gamma_n$ *is plotted versus* γ_n *and* z_n, *while in fig 2.4.1.*[b] $-\arg(R_n)$ *is plotted versus* γ_n *and* z_n. *Note that the scales of both* γ_n *and* z_n *are logarithmic.*

basic matrix is of order two. Thus, we have obtained an algorithm, which is most suitable for numerical implementation.

In terms of the coefficients $c_n(t)$, expressions (2.1.17). (2.1.18) and (2.119) can be written as ($\alpha = (q-1/2)\pi$, with q=1,2,3,...)

$$\rho(x,t) = e\Big|\sum_n c_n(t)\, \phi_n^{a(t)}(x)\Big|^2 , \qquad (2.4.12)$$

$$j(t) = s\,\frac{\pi e\hbar}{mL^2}\sum_{n=even}\left[\, |c_n(t)|^2\, n - |c_{n+1}(t)|^2\,(n+1)\,\right] \qquad \phi(2.4.13)$$

and

$$E(t) = \frac{\hbar^2\pi^2}{2mL^2}\sum_n |c_n(t)|^2\, n^2 , \qquad (2.4.14)$$

where s=1, if α reduced to the interval $[-\pi/2,3\pi/2]$, is $-\pi/2$ and s=-1 if α, reduced to the interval $[-\pi/2,3\pi/2]$, is $\pi/2$.

2.5. Self-induced phase-randomization and reversibility.

It was recently recognized by Lenstra and van Haeringen [8,9], that under certain suitable conditions a peculiar and unexpected sort of randomization effect shows up in the $c_n(t)$-coefficients, as a result of multiple matrix multiplications. To study this effect we have to examine the phase angles A_n and B_n, which are present in the transition matrix (2.4.9). It is convenient to express A_n and B_n in terms of the band index n. Therefore, we will introduce

$$\gamma_n = \gamma_{n_F} \frac{n_F}{n}; \qquad z_n = z_{n_F} \frac{n}{n_F}, \tag{2.5.1}$$

where γ_{n_F} and z_{n_F} denote the values of γ_n and z_n at the Fermi level n_F. In accordance with (2.4.4) we have

$$\gamma_{n_F} = \frac{2p^2mL}{eF\hbar^2\pi n_F}; \qquad z_{n_F} = \frac{\hbar^2\pi^2 n_F}{2mL^2p}. \tag{2.5.2}$$

The phase angles A_n and B_n can now be written as

$$A_n = \frac{\gamma_{n_F} z_{n_F}^2}{n_F}(n^2+1/12) + \gamma_{n_F} z_{n_F} \tag{2.5.3}$$

and

$$B_n = \frac{z_{n_F}\gamma_{n_F}}{2}\sqrt{1+(z_{n_F}\frac{n}{n_F})^2} + \frac{z_{n_F}\gamma_{n_F}}{2n}\ln\left(z_{n_F}\frac{n}{n_F} + \sqrt{1+(z_{n_F}\frac{n}{n_F})^2}\right) \tag{2.5.4}$$

For realistic parameter values, especially the A_n's can assume quite large values. For instance, with n_F>2000, $L=10^{-6}$ m, and F=1 V/m, the first term of A_n is about 5.10^6 for n's in the order on n_F.

The randomization effect of A_n is basically related to fact that if

n	$(A_n \bmod 2\pi)/2\pi$	$(B_n \bmod 2\pi)/2\pi$
1990	0.51779554	0.54644510
1991	0.20388677	0.02036348
1992	0.30177710	0.49428197
1993	0.81146652	0.96820056
1994	0.73295503	0.44211925
1995	0.06624264	0.91603805
1996	0.81132933	0.38995695
1997	0.96821512	0.86387595
1998	0.53689999	0.33779506
1999	0.51738396	0.81171428
2000	0.90966702	0.28563359
2001	0.71374917	0.75955301
2002	0.92963041	0.23347254
2003	0.55731075	0.70739216
2004	0.59679017	0.18131189
2005	0.04806869	0.65523172
2006	0.91114629	0.12915166
2007	0.18602299	0.60307169
2008	0.87269878	0.07699183
2009	0.97117366	0.55091207
2010	0.48144763	0.02483242

Table 2.5.1. The phaseangles A_n and B_n, reduced to the interval $[0,2\pi]$ and divided by 2π as a function the bandindex n. (γ_{n_F}=0.21, z_{n_F}=111. and n_F=2000)

we reduce the A_n's to the interval $[0,2\pi]$, they seem to form a random distribution of angles. This quasi-randomness is illustrated in table 2.5.1, where we show A_n and B_n (after reduction to the interval $[0,2\pi]$ and after dividing by 2π) in the case of γ_{n_F}=0.21, z_{n_F}=111. and n_F=2000. To illustrate that our set indeed behaves like a real random set we also calculated for the above-mentioned parameter values the various moments, $\left\langle \left[\frac{A_n \bmod 2\pi}{2\pi} \right]^m \right\rangle$, with m = 1,2,...,7 averaged over 1000 different n's. Within in accuracy of 10^{-3} they were equal to $(m+1)^{-1}$, which are the expected values for a random set in the interval [0,1].

n	$(A_n \bmod 2\pi)/2\pi$	$(B_n \bmod 2\pi)/2\pi$
1990	0.02083	0.01942
1991	0.27083	0.79400
1992	0.02083	0.56854
1993	0.27083	0.34310
1994	0.02083	0.11766
1995	0.27083	0.89222
1996	0.02083	0.66678
1997	0.27083	0.44136
1998	0.02083	0.21590
1999	0.27083	0.99046
2000	0.02083	0.76502
2001	0.27083	0.53958
2002	0.02083	0.31416
2003	0.27083	0.08870
2004	0.02083	0.86326
2005	0.27083	0.63782
2006	0.02083	0.41238
2007	0.27083	0.18696
2008	0.02083	0.96150
2009	0.27083	0.73608
2010	0.02083	0.51062

Table 2.5.2. The phaseangles A_n and B_n, reduced to the interval $[0,2\pi]$ and divided by 2π as a function the bandindex n. ($\gamma_{n_F}=\pi/10$, $z_{n_F}=100.$ and $n_F=2000$). Note that in this case the phases A_n do not randomize.

For some special choices of the parameters (e.g. $z_{n_F}=100$, $\gamma_{n_F}=\pi/10$ and $n_F=2000$, see table 2.5.2) no randomization occurs. More generally, in the presence of a delta-function potential it is always possible to choose parameter combinations in such a way that the set $\{A_n \bmod 2\pi\}$ constitutes a very restricted set of phases (2 in the above example) only. In such cases there is clearly no phase-randomization in the A_n's. This is an artifact of our delta-function potential model. For all other potentials the parameter p will become dependent on n. This can easily be understood if we recall that the p's showed up as Fourier components of the potential (see (2.3.2)).

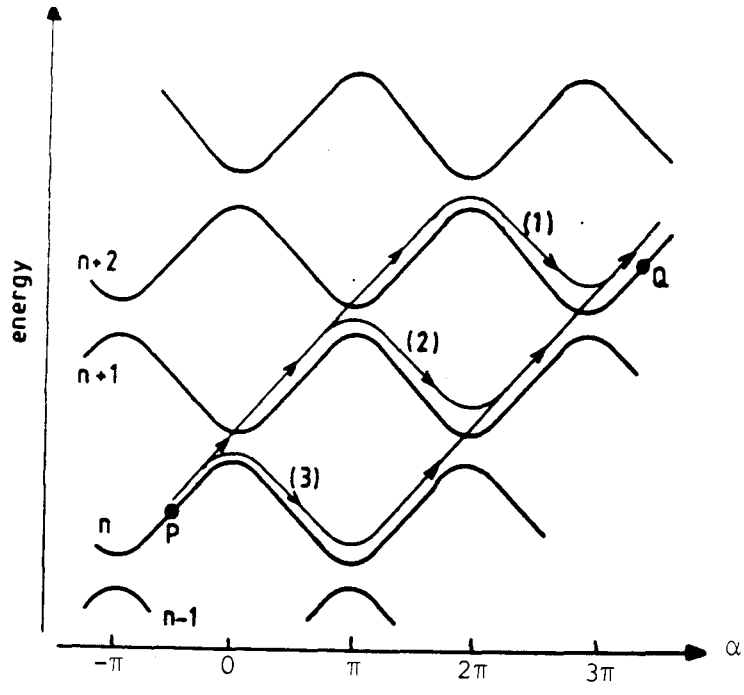

Fig.2.5.1. Detail of the energy spectrum; showing three different trajectories in (E,α)-space.

Some of the consequences of phase-randomization can be shown in the following way. Consider in the band structure, as indicated in fig 2.5.1, an electron starting in P with coefficient $c_P=1$ and collect all contributions to the coefficient c_Q. There is one contribution due to each trajectory connecting P and Q. The contributions of each trajectory will be denoted by $m^{(i)}$, where i labels the different trajectories as indicated in fig 2.5.1. In Q we have $c_Q=\sum_i m^{(i)}$. In the calculations of electronic quantities such as current and energy, we need all occupation numbers $|c_Q|^2$ in all different Q-points at a given time. In the above example we can write

$$|c_Q|^2 = \sum_i |m^{(i)}|^2 + \sum_{i \neq j} m^{(i)*} m^{(j)}, \qquad (2.5.5)$$

and this relation has a more general validity also. The whole idea is now that if the A_n's form a quasi-random set, the second term of (2.5.5) will lead to fluctuating (in time) contributions when substituted in expressions like (2.4.13) and (2.4.14), i.e., there will be an averaging effect in these quantities. Hence, apart from fluctuations, the qualitative (time-averaged) behaviour of the quantities will be correctly described by taking into account the first term of (2.5.5) only. Precise phase-relations, although conserved, appear to be less important, except in those exceptional cases in which phase randomization does not occur.

So far, the ideas still have to be numerically demonstrated, as will be done in section 3.1. We want to emphasize at this point that our system is deterministic and reversible in time. By deterministic we mean that, once the coefficients to start with are given, all coefficients at later times are determined. By reversible we mean that, if at a certain moment the field and the velocities are reversed, the time-evolution follows from then on the same pattern in opposite direction.

We will show numerically in section 3.1 that determinism and reversibility are not at all in contradiction with the above mentioned randomization effect. On the contrary, it illustrates ones more, that what we really have is quasi-randomness.

Now suppose, we do not know the deterministic rules which govern the time-evolution of the c_n's. Since the latter occur to us in a sense

as random and uncorrelated, it would be tempting to apply a statistical theory, such as Boltzmann's transport theory, in order to predict the current and energy development. Could our quasi-randomness play the same role as the assumption of "Molecular chaos" or the "Stosszahlansatz" in the Boltzmann equation usually does? If so, what happens then with the reversible nature of our system?

In chapter 4 we will return to these questions and develop a Boltzmann-like theory for our system, making the assumption of complete phase-randomization.

3. NUMERICAL RESULTS AND DISCUSSION.

In this chapter we present the numerical results obtained. With the aid of the transition matrices (2.4.9) we will calculate the coefficients $c_n(t)$ at successive discrete times

$$t = \frac{\hbar}{eFL}\alpha = \frac{\pi\hbar}{eFL}(q-1/2) \qquad (3.0.1)$$

with the number of time steps q=1,2,3,.. .

Once we have numerical values for the $c_n(t)$'s the quantities of interest, such as the charge-density distribution, the electrical current and the total energy, can be calculated. As the initial condition for each electron we will start in an eigenstate, i.e. $c_n(q=0) = \delta_{nn_o}$, where n_o is a fixed given band index. If we want to study more electrons we repeat the above-described procedure - taking different n_o's of course, in order to satisfy the Pauli-principle - and add the corresponding contributions to the quantities of interest. We stress, that it is <u>not</u> correct to calculate many-electron properties by filling the bands in advance and perform one calculation, because then we would not start in a proper many-electron eigenstate, but, apart from normalization, in a mixed single-electron state.

We have always taken an <u>even</u> number of electrons, initially occupying neighbouring bands. This is convenient in order to avoid irrelevantly high initial values of the current. Starting with two electrons (or an even number) in neighbouring bands, the one-electron contributions will be pairwisely highly compensating, leading to an

almost vanishing initial current. However, most of the results to be presented are insensitive to whether an odd or an even number of electrons is considered, that is, after some time. The only reason for taking an even number of electrons is to avoid weird-looking pictures.

We will study the electrons near the Fermi level (with bandindex n_F). In real rings, n_F equals the number of participating electrons. Hence we must think of $1 \cdot 10^5$, or so. However, we will consider in the calculations values of n_F between 200 and 400. This yields a considerable reduction in computation time. We claim, that the essential features, studied here, are unaltered by this drastic reduction of n_F.

Furthermore we will restrict ourselves to such values of γ_n and z_n, that R_n may be approximated by $\exp(-\pi\gamma_n/4)$. This implies that the band gaps are not too small and the fields are not too strong

3.1 The current.

In fig. 3.1.1 the result of a current calculation is shown for two electrons with $n_F = 300$, $\gamma_{n_F} = 0.0255$ and $Z_{n_F} = 100$. The electrons initally occupy the bands with n = 260 and 261, respectively. One may recognize that after about 20 time steps the current more or less saturates, albeit that the fluctuations around the "time-independent" value, i.e. 35 $\pi e\hbar/mL^2$, are enormous. These fluctuations, however, considerably reduce as the number of electrons is increased. This is shown in fig. 3.1.2, where initially all bands with $220 \leq n \leq 299$ are filled (i.e. there are 80 participating electrons). The short-time fluctuations have almost disappeared, except for a sort of ripple, the

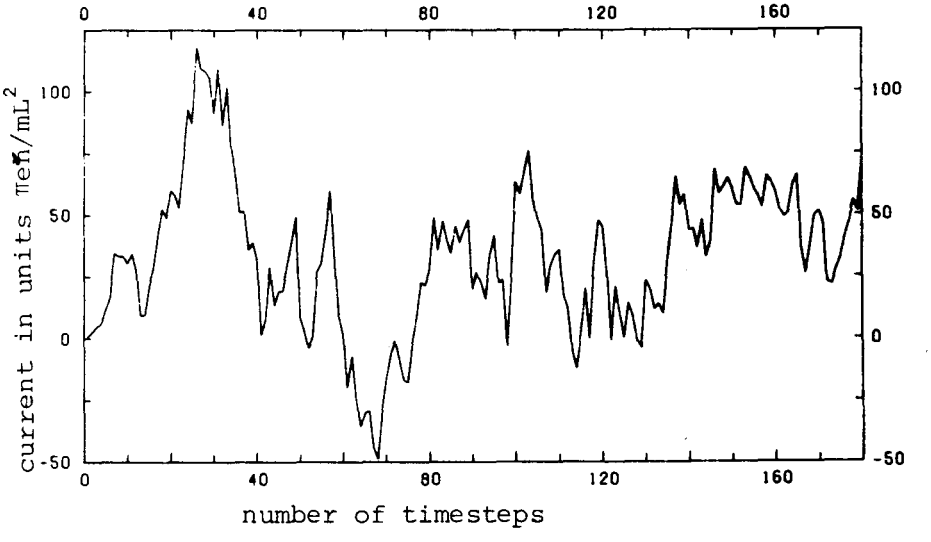

Fig.3.1.1. Current as a function of the number of time-steps q (q is introduced in (3.0.1)). No regularity is observed at first sight, but if we increase the number of electrons, one recognizes saturation (see fig 3.1.2) (γ_{n_F}=0.0255, z_{n_F}=100., n_F=300, and the initially occupied bands are given by n=260,261)

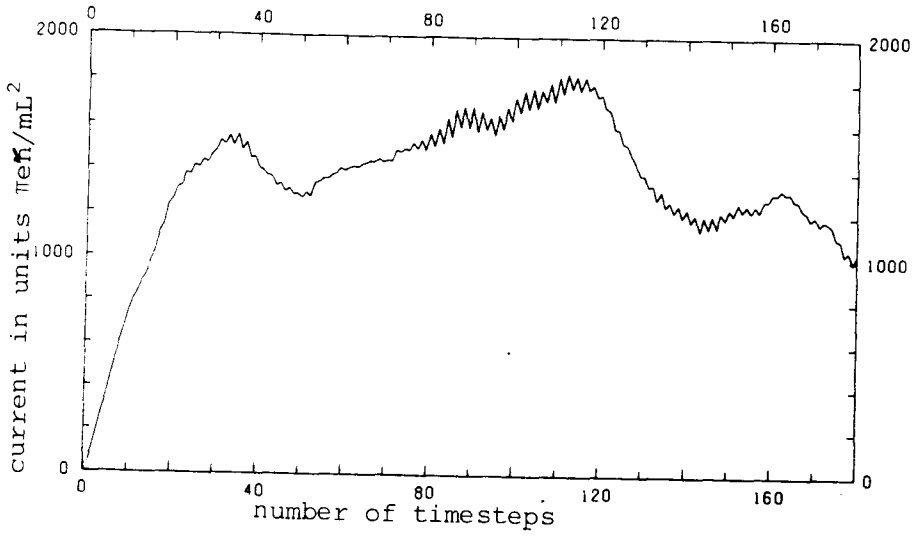

Fig.3.1.2. Current as a function of the number of time steps. Saturation is clearly visible now. However, some fluctuations still exist. (γ_{n_F}=0.0255, z_{n_F}=100., n_F=300, *and the initially occupied bands are given by* $220 \leq n \leq 299$)

period of which is fully compatible with the 2π-period in α. A persisting fluctuation, with typical period $\Delta\alpha \cong 30\pi$ is present, the origin of which is not yet clear to us. This might be a long-time memory effect related to persisting correlations in the phase-angles, which, as we recall, are only seemingly random.

One also notices by comparing fig. 3.1.1 and 3.1.2, that the current is fairly linear in the amount of electrons. In a paper by Lenstra and van Haeringen [9], it has already been shown, that the saturation value is also roughly linear in the applied field (which is proportional to $\gamma_{n_F}^{-1}$, see also fig. 4.3.2). Both the linearity in the applied field and the linearity in the number of electrons strongly suggests "ohmic" or even "resistive" behaviour.

Usually, resistance is assigned to dissipative systems only. Our system is clearly not dissipative in the sense of energy dissipation. Still, it seems to us that is develops resistive-like behaviour, which is due to phase-randomization, and not to energy dissipation. Instead, we might introduce here the notion of dissipation of phase information. To illustrate how the phase-randomization is responsible for the resistive behaviour, we show in fig. 3.1.3 the current development for three closely spaced γ_{n_F}'s. In one case the current does not saturate, while in the other cases saturation does occur. The case in which

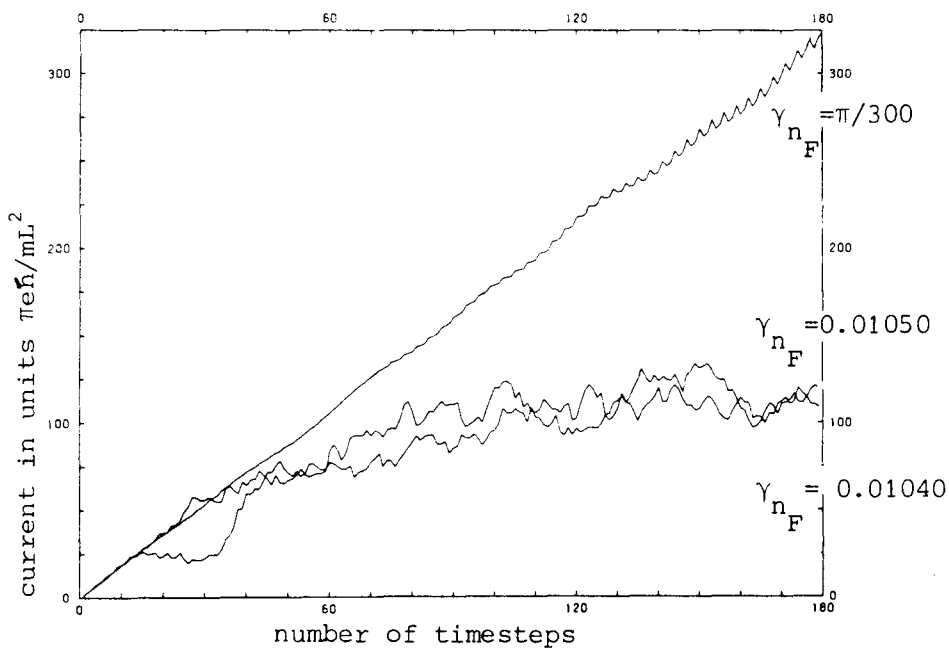

Fig.3.1.3. Current response for three closely spaced γ_{n_F}*'s. For* $\gamma_{n_F}=\pi/300$ *no randomization and no saturation occurs, while in the other cases, both randomization and saturation occur.* ($z_{n_F}=100.$, $n_F=200$, *and the initially occupied bands are given by n=198,199*)

saturation is not happening, corresponds to $\gamma_{n_F} = \pi/300$, $Z_{n_F} = 100$ and $n_F = 200$, and one easily verifies that the set of phase angles $\{A_n \bmod 2\pi\}$ consists of four elements only. For the two other values of γ_{n_F} this set consists in principle of a non-restricted number of irregularly spaced angles.

In the absence of saturation small oscillations are present in the current development. These oscillations are due mainly to the fact that γ_n and z_n are dependent on n. If we remove this n-dependence, i.e. put γ_n and z_n equal to constants, the oscillations significantly reduce.

Already in 1970, Landauer [1] introduced the concept of phase-randomness of wave functions in order to derive a formula for the resistance of a one-dimensional wire in between two heat baths (or "Ohmic" contacts), where the electrons in the wire experience elastic scattering only. In Landauer's derivation the randomization of the phases is essential and the idea was that the two heat baths took care of that. Indeed, Landauer's theory strongly suggests that the introduction of at least one heat bath is really needed if one attempts to assign resistance to a system in which scattering of electrons is fully elastic. It seems to us that the quasi-randomness of the phases in our deterministic system plays a similar role as real randomness does in Landauer's system. According to our view, the Landauer formula should be applicable to non-dissipative (in the above sense) systems also. It would be worthwile to investigate this further.

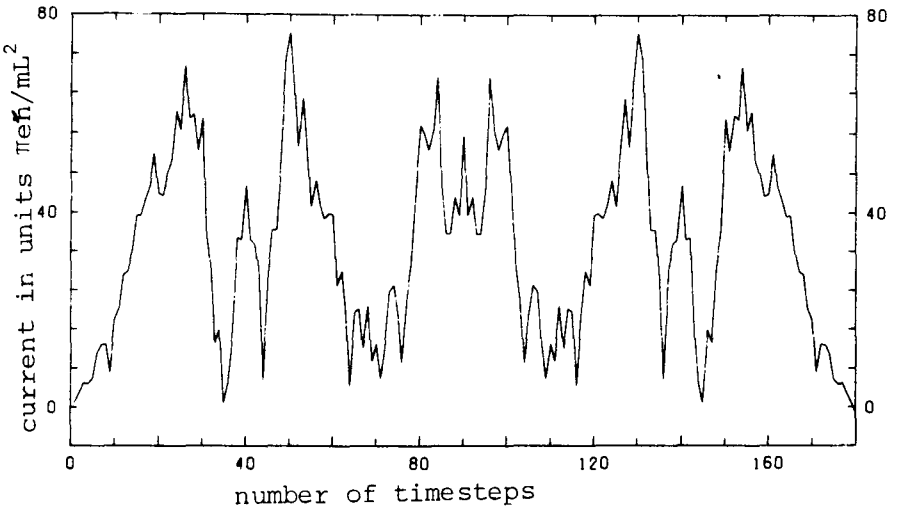

Fig.3.1.4. Current development. After 90 time steps the field and the velocities are reversed. This calculation demonstrates the reversibility of our system. (γ_{n_F}=0.0255, z_{n_F}=100., n_F=200, *and the initially occupied bands are given by n=198,199*)

In fig. 3.1.4 we demonstrate the reversibility of our system. We reversed the electric field and the velocities after 90 time steps, whereafter the current returns to its initial value, following exactly the original time development. This calculation also demonstrates, that round-off errors play no role of importance, as a randomization mechanism. Since the coefficients $c_n(t)$ might be more sensitive to round-off errors, we also checked them after reversing the field. Starting with $c_1 = \delta_{11}$, , ultimately only a probability of 1.10^{-8} had appeared in all other bands together. We estimate that this loss of significant numbers can influence the qualitative behaviour only after performing more than 10^5 time steps, i.e. at least 10^3 times as many as was done here.

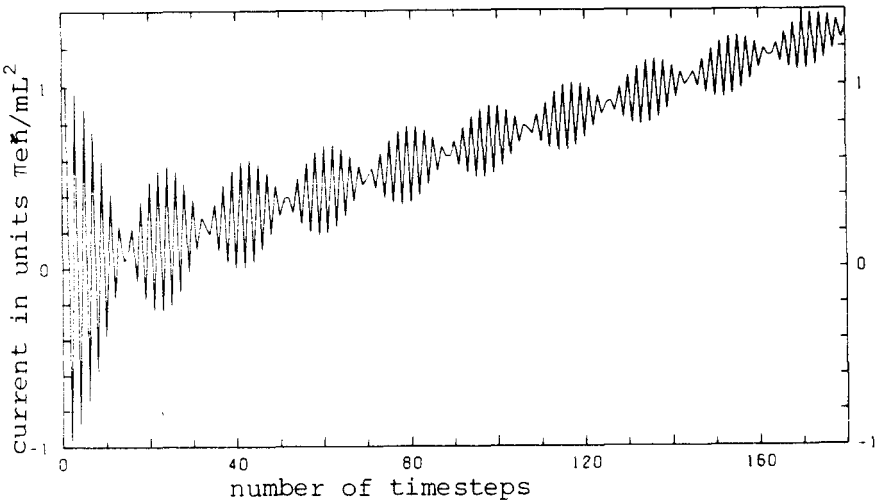

Fig.3.1.5. Current development in the case of a very weak field. The rapid fluctuaions with period 2 are Josephson-oscillations. The slow beats with period 36 are the subtle results of the small but non-vanishing tunneling-probabilities and coherent interference effects. ($\gamma_{n_F}=\pi$, $z_{n_F}=100.$, $n_F=200$, *and the initially occupied bands are given by* $n=198,199$)

In fig. 3.1.5 the current-development in the case of a very weak field without phase-randomization is shown ($\gamma_{n_F}=\pi$, $z_{n_F}=100$ and $n_F=200$). In this case the electrons have only a probability of 0.7% per scattering event to tunnel to another band (i.e. the Zener-tunneling probability). If the electrons would remain in their bands, the velocity would be an oscillating function of time. In fact, we would then have the Josephson-like oscillations, which were predicted by Buttiker, Imry, and Landauer [4]. The oscillations with period $\Delta\alpha=2\pi$ in fig 3.1.5 are these Josephson-like oscillations. However, we see more interesting things in the figure: The average current is increasing with time and we see beats with a period of $\Delta\alpha=36\pi$ (equivalent with $\Delta q=36$). This numerical result shows that Zener-tunneling, although very weak, cannot

be neglected, since it introduces coherent interference effects, such that after as few as 10 time steps (i.e. 5 periods of α) drastic deviations from the expected simple Josephson-like phenomena occur.

3.2. Charge-density distribution and energy.

To calculate the charge-density distribution we use (2.4.12). In fig 3.2.1 the charge-density distribution along the wire for two electrons is shown at succesive times corresponding to $\alpha=-\pi/2$, $9\pi/2$, $19\pi/2,\ldots,$ $49\pi/2$. One notices that, initially, the charge is homogeneously distributed over the wire, while as time proceeds the distribution seems to randomize more and more.

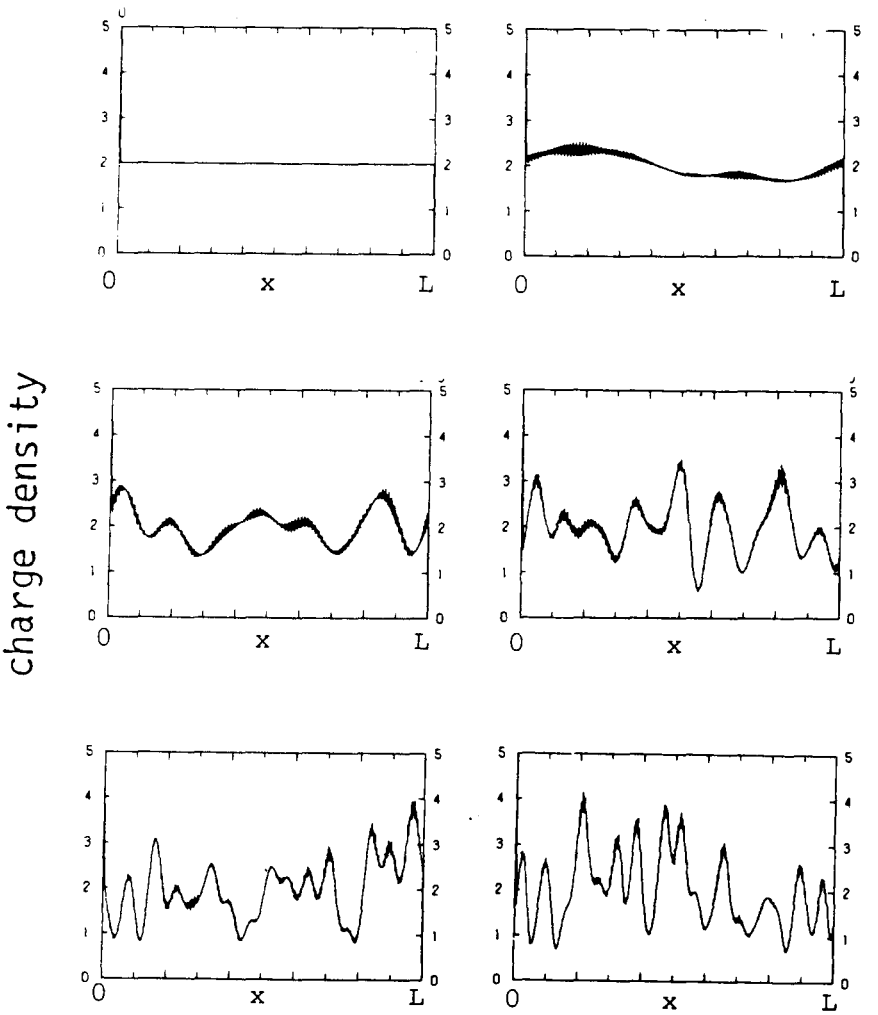

Fig.3.2.1. Charge distribution of two electrons at succesive times $q=0,5,10,\ldots,25$. *Self-induced phase-randomization leads to charge-density randomization.* ($\gamma_{n_F}=0.0255$, $z_{n_F}=100.$, $n_F=200$, *and the initially occupied bands are given by* $n=198,199$)

Fig 3.2.2 illustrates that the charge is moving indeed. Here the charge-distribution is shown at times t corresponding to values of α between 19.500π and 19.508π at α-intervals $\Delta\alpha=10^{-3}\pi$.

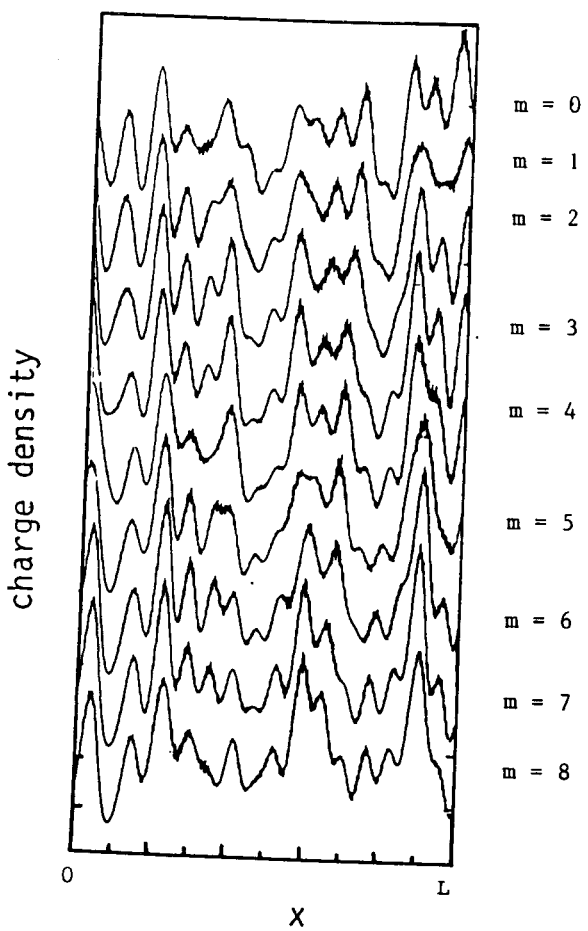

Fig.3.2.2. Illustrating the flow of charge due to two electrons. Charge distributions are shown at q=20+mΔq, where Δq=0.001 and m=0,1,2,....,8. (γ_{n_F}=0.0255, z_{n_F}=100., n_F=200, and the initially occupied bands are given by n=198,199)

To calculate the energy we use (2.4.14). In fig. 3.2.3 and 3.2.4 the current and the energy are shown as functions of time for n_F=2000, γ_{n_F}=0.0255 and z_{n_F}=100. In fig. 3.2.3 and 3.2.4 a special feature of our system is demonstrated, whether the current saturates or not, the total energy increases. This implies that the system does not reach a stationary state. Usually dissipative systems (in contrast with non-dissipative sytems, like ours) do reach a stationary state. The increasing of the energy can be explained by using a variant of Ehrenfest's theorem,

$$\frac{d}{dt} E_{tot} = FL\ j(t), \qquad (3.2.1)$$

the proof of which can easily be given: One calculates the total time-derivative of the hamiltonian and uses the time-dependent Schrodinger equation (2.1.1) After some rearrangements one recognizes the current-operator, after which (3.2.1). follows. Note that (3.2.1) is an exact relation, which can also be used to check the numerical consistency.

We will come back to the typical non-stationary aspect as demonstrated by the system's ever-increasing energy ("heating" up of the electrons) in chapter 4, in the context of a Boltzmann-type of equation

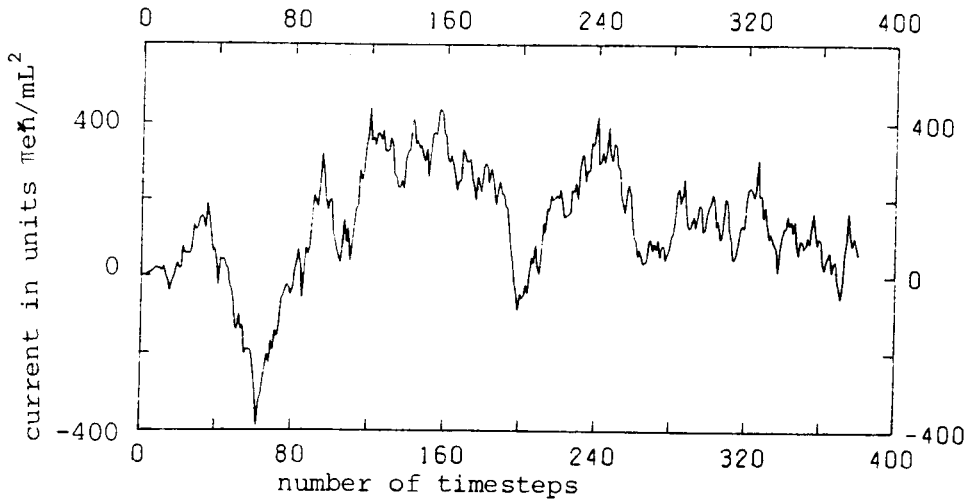

Fig.3.2.3. Current development as a function of time. (γ_{n_F}=0.0255, z_{n_F}=100., n_F=2000, and the initially occupied bands are given by n=1998,1999).

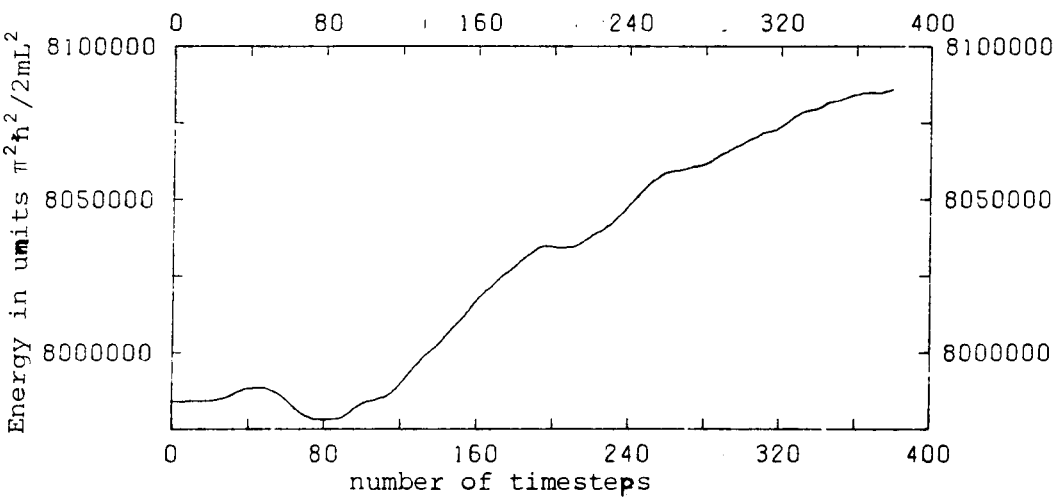

Fig.3.2.4. Energy development for the same case for which the current is shown in fig.3.2.3.

3.3. The "entropy".

In this section we will return to the quasi-randomness of the phases. In a system with stochastic randomization, entropy can be considered as a measure for the "amount of disorder". The entropy σ in a quantummechanical system is defined by

$$\sigma = \mathrm{Tr}[\rho(t)\ln\rho(t)], \tag{3.3.1}$$

where $\rho(t)$ is the socalled "statistical" or "density" matrix, which, in principle, carries all relevant information of the system in it. The operator $\ln\rho$ is the operator, whose eigenvalues are equal to the logarithms of the eigenvalues of ρ and whose eigenvectors coincide with those of ρ.

In our system, the initial state vectors are eigenvectors, which makes the initial entropy zero. However the entropy (3.3.1.) will remain zero also for later times, because the unitary time-evolution operator will carry the system over in pure states.

Although the proper entropy (3.3.1) is zero, in agreement with the lack of real randomness, the quasi-randomness nevertheless suggests that an alternative definition of entropy might be useful in quantifying the amount of quasi-randomness. We will therefore introduce the quantity S (which we will also refer to as "entropy") defined by

$$S \equiv \sum_{\text{electrons}} \sum_{n} |c_n|^2 \ln|c_n|^2 \tag{3.3.2}$$

A remark has to be made here. One must realize that (3.3.2) defines an entropy which is fixed to the "stationary" states of which the c_n's are

the corresponding probability amplitudes. Of course, such a "subjective" definition of entropy can only have a very restricted usefulness, i.e. only in situations, where one choice of "stationary" states as a basis is physically more meaningful than any other choice of basis states.

In fig. 3.3.1 we show the "entropy" for the same case, for which the current and energy are shown in fig. 3.2.3 and 3.2.4. The shape of the entropy curve is representative for all calculations performed. Note that the horizontal scale is a logaritmic one. In all cases considered, the entropy had the $\int$-shape, where the position of the first kink roughly corresponds to the typical time interval (to be interpreted as the "collision time") after which current saturation occurred. The meaning of the second kink (in the figure situated around 10^2) is

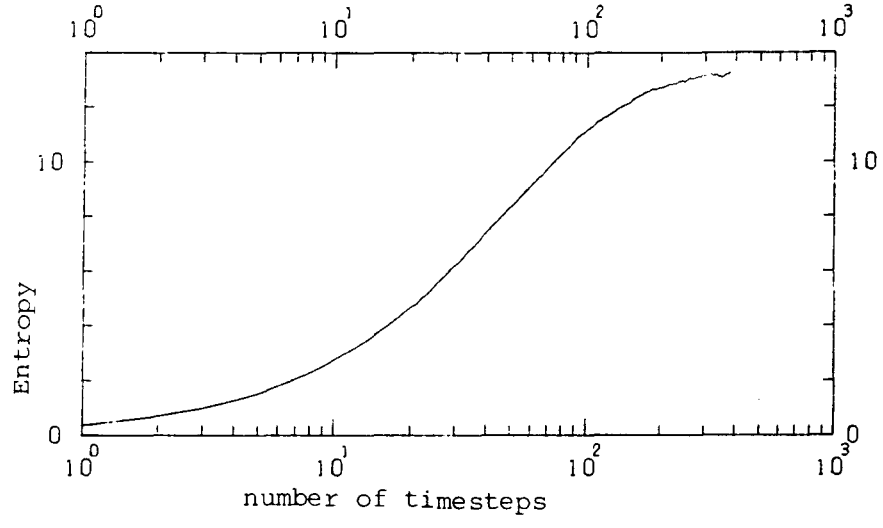

Fig.3.3.1. The "entropy" as a function of the number of time steps for the same parameters as used to calculate the current and energy in fig.3.2.3. and 3.2.4.

obscure to us. It seems to indicate the presence of a second typical timescale, which is not obvious from observations of the current behaviour.

Except for very special cases (e.g. the time-reversed case of fig. 3.1.4) we have never seen the entropy to decrease. However, the increase rate of entropy shows clear dips as a function of γ_{n_F} precisely at those values where phase-randomization and current saturation is absent.

We do not have a theory around, or a justification for, the introduction of the entropy. It must be seen as no more than a first step on a way towards a complete and elaborate theory.

By construction, our entropy is additive in the number of electrons, in contrast to the real entropy of a system of non-interacting fermions in thermal equilibrium. The reason for this is, that our subjective definition does not take proper account of the indistinguishability of the electrons, whereas the real entropy does. We will return to this problem in chapter 4, where we will derive a Boltzmann equation to describe global properties of our system, and after solving it, calculate the usual Boltzmann entropy.

4. STATISTICAL DESCRIPTION BASED ON A BOLTZMANN EQUATION.

4.1. Derivation of a Boltzmann equation.

In the previous chapters we have used the Schrodinger equation to describe the dynamics of electrons in our system. If we want to study the behaviour of the electrons only roughly, the Schrodinger equation has turned out to be rather cumbersome. By making use of the phase-randomization effect, the theory of which has already been treated in section 2.5, we will derive a Boltzmann-type of equation.

We start at time τ, exactly in between two degeneracies (see fig 4.1.1), with known coefficients $c_n(\tau)$ of the wave function $\Psi(x,\tau)=\sum_n c_n(\tau)e^{ik_n x}$, where k_n is the wave vector, belonging to band n at time τ. k_n will be specified lateron. We will relate the c_n-coefficients somehow to an occupation probability, whose time evolution can be described in a Boltzmann-like manner. We will therefore first calculate the c_n's during one period of time, corresponding to one period of α, i.e. $\tau \leq t \leq \tau+2\pi\hbar/eFL$. Using (2.4.9), one easily calculates the coefficients at time $\tau+2\pi\hbar/eFL$, (denoted by c_n''). We then have

$$c''_{n+1} = \left[e^{-i(A_n+A_{n+1})} \{ -e^{-i(B_n)} R_n T_{n+1} c_{n+2} + e^{-i(B_n-B_{n+1})} R_n R^*_{n+1} c_{n+1} \} + \right.$$
$$\left. + e^{-i(A_{n-1}+A_n)} \{ e^{-i(B_{n-1})} T_n R_{n-1} c_n + T_n T_{n-1} c_{n-1} \} \right] \qquad (4.1.1)$$

and

$$c''_n = \left[e^{-i(A_n+A_{n+1})} \{ T_n T_{n+1} c_{n+2} - e^{i(B_{n+1})} T_n R^*_{n+1} c_{n+1} \} + \right.$$
$$\left. + e^{-i(A_{n-1}+A_n)} \{ e^{-i(B_{n-1}-B_n)} R^*_n R_{n-1} c_n + e^{i(B_n)} R^*_n T_{n-1} c_{n-1} \} \right], \qquad (4.1.2)$$

where $c_n = c_n(\tau)$.

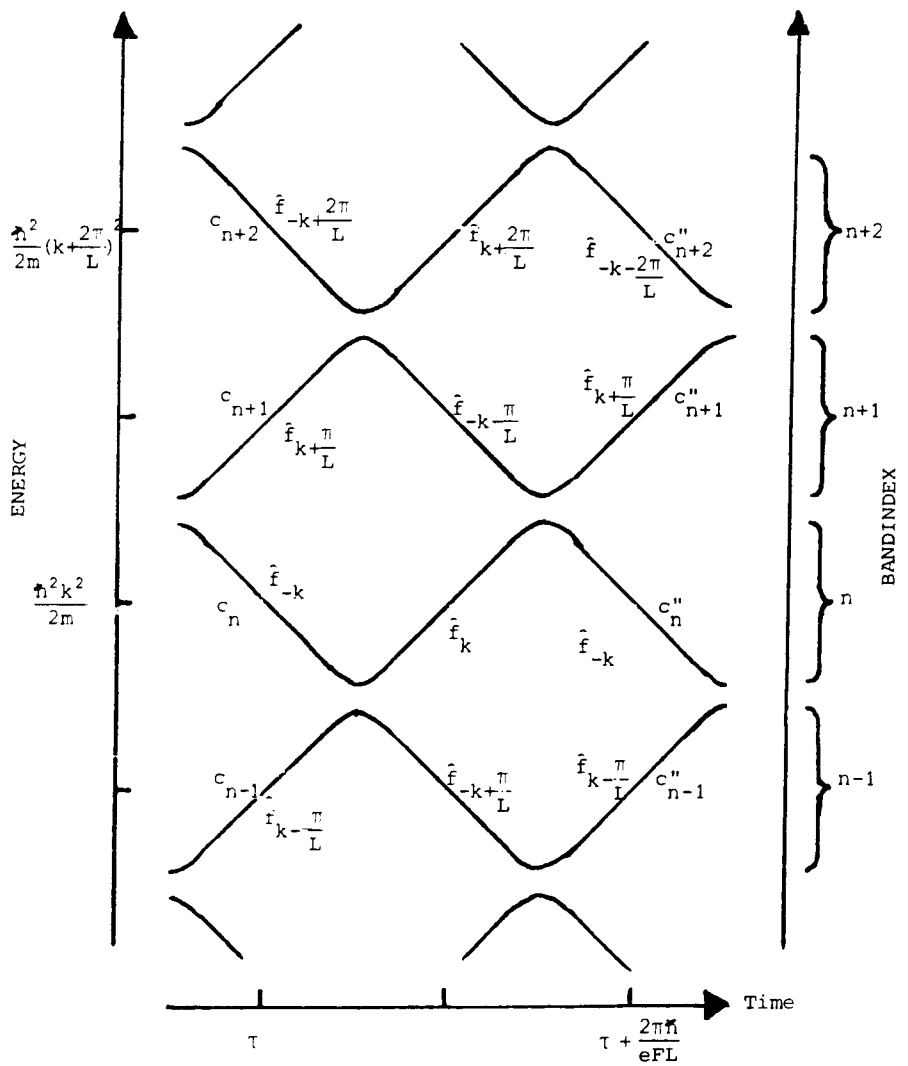

Fig.4.1.1. Detail of the energy spectrum as a function of time ($=\frac{\kappa}{eFL}\alpha$) *Indicated is the correspondence between the probabilities* $f_k(t)$ *and the coefficients* $c_n(t)$.

We now introduce a probability distribution $\hat{f}_{k_n}(t)$ for an electron to have the velocity $\hbar k_n/m$ at time t. The time t will be chosen in between two degeneracies. As we have seen before, at these moments an electron has an almost sharp velocity (or momentum), because the corresponding wave functions can then be represented by one plane wave. We define

$$\hat{f}_{k_n}(t) \equiv |c_n(t)|^2, \tag{4.1.3}$$

where

$$k_n = \mathrm{sgn}\left[\partial\epsilon_n^{\alpha(t')}/\partial t'\Big|_{t'=t}\right] (n+1/2)\,\frac{\pi}{L}, \tag{4.1.4}$$

The sign of k_n indicates the direction of the velocity. For example, for the band with index n+1 and at time τ or $\tau+2\pi\hbar/eFL$ the velocity is positive, while for the same band and at time $\tau+\pi\hbar/eFL$ the velocity is negative. We will denote the k_n belonging to band n with k (see fig. 4.1.1).

If we make the simplifying assumption that the T_n's and the R_n's are independent of n and have magnitudes T and R, one easily derives from (4.1.1) and (4.1.2) that

$$|c''_{n+1}|^2 = R^2T^2|c_{n+2}|^2 + R^4|c_{n+1}|^2 + T^2R^2|c_n|^2 + T^4|c_{n-1}|^2 + g_{n+1}(A_{n-1},A_{n+1},B_n,B_{n+1},B_{n-1},R,T,c_{n-1},c_n,c_{n+1},c_{n+2}) \tag{4.1.5}$$

and

$$|c''_n|^2 = T^4|c_{n+2}|^2 + T^2R^2|c_{n+1}|^2 + R^4|c_n|^2 + R^2T^2|c_{n-1}|^2 + g_n(A_{n-1},A_{n+1},B_n,B_{n+1},B_{n-1},R,T,c_{n-1},c_n,c_{n+1},c_{n+2}), \tag{4.1.6}$$

where g_{n+1} and g_n are known functions, which in contrast to the other

terms in (4.1.5) and (4.1.6) heavily depend on the A_n's and B_n's (explicitly through $A_{n+1}, A_{n-1}, B_n, B_{n+1}$ and B_{n-1}, and implicitly through the A_n and B_n-dependence of the c_n's). If the phases A_n are random, the functions g_n heavily fluctuate. By this we mean that at fixed t, g_n is an irregular function of n, fluctuating around zero in a seemingly random way, while the same applies for g_n at fixed n as a function of t. This can be seen if one looks more closely at the exact expressions for, e.g., g_{n+1}, that is,

$$\begin{aligned} g_{n+1} = 2\,\mathrm{Re}\,\Big[& -e^{-i(B_{n+1})}\, R\, T\, R^*\, R\, c_{n+2}\, c^*_{n+1} + \\ & - e^{-i(B_n+A_{n+1}-A_{n-1}-B_{n-1})}\, R\, T\, T\, R^*\, c_{n+2}\, c^*_n + \\ & - e^{-i(B_n+A_{n+1}-A_{n-1})}\, R\, T\, T\, T\, c_{n+2}\, c^*_{n-1} + \\ & + e^{-i(B_n-B_{n+1}-B_{n-1}+A_{n+1}-A_{n-1})}\, R\, R^*\, T\, R^*\, c_{n+1}\, c^*_n + \\ & + e^{-i(B_n-B_{n+1}+A_n-A_{n-1})}\, R\, R^*\, T\, T\, c_{n+1}\, c^*_{n-1} + \\ & + e^{-i(B_n)}\, T\, R\, T\, T\, c_n\, c^*_{n-1}\,\Big]. \end{aligned} \tag{4.1.7}$$

Using the definition of the $\hat{f}_k(t)$ (4.1.3) and the equality $(|R|^2+|T|^2)^2=|R|^4+|T|^4+2|RT|^2=1$ expressions (4.1.5) and (4.1.6) lead to

$$\begin{aligned} & \hat{f}_{k+\pi/L}(\tau+2\pi\hbar/eFL)-\hat{f}_{k+\pi/L}(\tau)+T^4[\hat{f}_{k+\pi/L}(\tau)-\hat{f}_{k-\pi/L}(\tau)]+ \\ & \qquad -|RT|^2[\hat{f}_{-k-2\pi/L}(\tau)+\hat{f}_{-k}(\tau)-2\hat{f}_{k+\pi/L}(\tau)] = g_{n+1} \end{aligned} \tag{4.1.8}$$

and

$$\begin{aligned} & \hat{f}_{-k}(\tau+2\pi\hbar/eFL)-\hat{f}_{-k}(\tau)-T^4[\hat{f}_{-k-2\pi/L}(\tau)-\hat{f}_{-k}(\tau)]- \\ & \qquad -|RT|^2[\hat{f}_{k+\pi/L}(\tau)+\hat{f}_{k-\pi/L}(\tau)-2\hat{f}_{-k}(\tau)] = g_n \end{aligned} \tag{4.1.9}$$

The left-hand sides of (4.1.8) and (4.1.9) strongly suggest a Boltzmann-like equation, while the right hand-sides represent fluctuating functions of time. The time scales of these fluctuations are

of the order of several periods of α. If we average $\hat{f}_k(t)$ over several different but closely spaced t's and k's, we are able to define a new smooth function, $f_k(t)$, which can be considered as continuous in both k and t. Hence k and t need no longer be restricted to special values only.

It is now possible to associate the average of $\hat{f}_k(\tau-2\pi\hbar/eFL)-\hat{f}_k(\tau)$ with a first derivative with respect to time and the average of $\hat{f}_k(\tau)-\hat{f}_{k-2\pi/L}(\tau)$ with a first derivative with respect to k. The definitions of the partial derivatives are given by

$$\frac{\partial f_k(t)}{\partial t} \equiv \frac{eFL}{2\pi\hbar} < \hat{f}_k(\tau+2\pi\hbar/eFL) - \hat{f}_k(\tau) > \qquad (4.1.10)$$

and

$$\frac{\partial f_k(t)}{\partial k} \equiv \frac{L}{2\pi} < \hat{f}_k(\tau) - \hat{f}_{k-2\pi/L}(\tau)>, \qquad (4.1.11)$$

where < a > denotes the mean value of the function "a" averaged over a several closely spaced k's and t's. If we average over a sufficiently large number of g_n's, its mean value will go to zero (the phases A_n are assumed to be random). If we apply the definitions (4.1.10) and (4.1.11) and take the $< g_n >$'s zero, expressions (4.1.8) and (4.1.9) can be written as

$$\frac{\partial f_k(t)}{\partial t} = -\frac{eF}{\hbar} T^4 \frac{\partial f_k(t)}{\partial k} - \frac{eFL}{\pi\hbar} |R|^2T^2 [f_k(t)-f_{-k}(t)] \qquad (4.1.12)$$

and

$$\frac{\partial f_{-k}(t)}{\partial t} = \frac{eF}{\hbar} T^4 \frac{\partial f_{-k}(t)}{\partial k} + \frac{eFL}{\pi\hbar} |R|^2T^2 [f_k(t)-f_{-k}(t)] \qquad (4.1.13)$$

If we finally introduce an effective field F_{eff}

$$F_{eff} \equiv F\, T^4 \qquad (4.1.14)$$

and the backscattering rate W

$$W \equiv \frac{eFL}{\pi\hbar} |R|^2 T^2 \tag{4.1.15}$$

we obtain the Boltzmann equations

$$\frac{\partial f_k(t)}{\partial t} = - \frac{eF_{eff}}{\hbar} \frac{\partial f_k(t)}{\partial k} - W [f_k(t)-f_{-k}(t)] \tag{4.1.16}$$

and

$$\frac{\partial f_{-k}(t)}{\partial t} = \frac{eF_{eff}}{\hbar} \frac{\partial f_{-k}(t)}{\partial k} + W [f_k(t)-f_{-k}(t)] \tag{4.1.17}$$

We want to emphasize that (4.1.16) and (4.1.17) can only give a rough description of the behaviour of our system. More specific, it cannot be expected that results of e.g. a current calculation based on the integration of (4.1.16) and (4.1.17) will show fluctuating behaviour as observed in fig. 3.1.1 and 3.1.2. What we in fact hope is that the present theory will predict correct time-averaged versions of the exact results of chapter 3.

It is stressed that we assumed that the T_n's and the R_n's were independent of n, i.e. of the energy of the electrons. Not making this assumption would imply that both the effective field and the backscattering rate become energy dependent.

4.2. Non-stationary solution of the Boltzmann equation.

To solve the Boltzmann equation (4.1.16) for $f_k(t)$ we will first derive an analytic solution for the function $g_k(t)=f_k(t)-f_{-k}(t)$. Lateron we will use the expression for $g_k(t)$ in order to obtain an analytic expression for the $f_k(t)$. In a paper by Lenstra and van Haeringen [6] a method is given to obtain the solution for the $g_k(t)$, by which, in principle, $g_k(t)$ can be solved for every time t. They only give the solutions for $t<\hbar k_F/eF$ (k_F is the absolute value of k at the Fermi level).Following the above-mentioned method, we differentiate expressions (4.1.16) and (4.1.17) with respect to t and subtract the obtained expressions. Using (4.1.16) and (4.1.17) again, we arrive at the homogeneous damped wave equation

$$\left[\frac{\partial^2}{\partial t^2} + 2W \frac{\partial}{\partial t} - \frac{e^2F^2}{\hbar^2} \frac{\partial^2}{\partial k^2} \right] g_k(t) = 0, \qquad (4.2.1)$$

where we replace F_{eff} by F.

As the initial conditions at t=0 ,we shall put $f_k(0)$

$$f_k(0) = \begin{cases} 1 & \text{for } |k|<k_F \\ 0 & \text{for } |k|>k_F. \end{cases} \qquad (4.2.2)$$

Note that this corresponds to a situation, in which all states with energies below the Fermi energy are occupied by electrons and all other levels are empty. This is different from the initial values, used in chapter 3, where only a few energy levels were occupied by electrons. However, as far as the energy and the current are considered this is no problem as we will see in section 4.3. For the entropy it makes quite a difference (see also section 4.3).

To solve (4.2.1) we use the transformation

$$g_k(t) = \int_{-\infty}^{\infty} dx\, e^{ikx}\, \hat{g}_x(t), \tag{4.2.3}$$

and derive expressions for $\hat{g}_x(t)$ (see for a precise derivation [10]). This yields for $g_k(t)$

$$g_k(t) = \frac{eF}{\hbar} \int_{-\infty}^{\infty} dx \left[\sinh(\sqrt{W^2 - e^2F^2x^2/\hbar^2}\; t)\, \frac{e^{i(k-k_F)x - Wt} - e^{i(k+k_F)x - Wt}}{\sqrt{W^2 - e^2F^2x^2/\hbar^2}} \right] \tag{4.2.4}$$

for $t>0$. After performing the integration [11] the solution of (4.2.1) can be written as

$$g_k(t) = \tilde{g}_{k-k_F}(t) - \tilde{g}_{k+k_F}(t), \tag{4.2.5}$$

where the functions $\tilde{g}_k(t)$ are given by

$$\tilde{g}_k(t) = \begin{cases} e^{-Wt}\, I_o[W\sqrt{t^2 - \hbar^2k^2/e^2F^2}] & \text{if } |k| < eFt/\hbar \\ 0 & \text{if } |k| > eFt/\hbar, \end{cases} \tag{4.2.6}$$

with I_o the modified Besselfunction of order zero.

Since we have an expression for $g_k(t)$, the Boltzmann equation (4.1.16) can be written as the <u>inhomogeneous</u> linear partial differential equation

$$\frac{\partial f_k(t)}{\partial t} + \frac{eF}{\hbar} \frac{\partial f_k(t)}{\partial k} = -W\, g_k(t), \tag{4.2.7}$$

to be solved with the initial values (4.2.2)

To solve (4.2.7) we will use the transformation

$$\left.\begin{aligned} k &= q + eFs/\hbar \\ t &= s \end{aligned}\right\} \tag{4.2.8}$$

One easily verifies that the functions $h_q(s)$ defined by

$$h_q(s) \equiv f_{q+eFs/\hbar}(s) \tag{4.2.9}$$

satisfies

$$\frac{\partial h_q(s)}{\partial s} = - W\, g_{q-eFs/\hbar}(s) \equiv M_q(s) \qquad (4.2.10)$$

Since q is only a parameter in (4.2.10), we can solve (4.2.10) by integration. If we also use the inverse of (4.2.8), we obtain for $f_k(t)$

$$f_k(t) = \left[\; h_q(0) + \int_0^s ds'\, M_q(s') \; \right] \Bigg|_{\substack{s = t \\ q = k - eFt/\hbar.}} \qquad (4.2.11)$$

This procedure is equivalent to integrating the original differential equations along the curve $k=q+eFt/\hbar$ for $-\infty<q<\infty$ (see fig. 4.2.1).

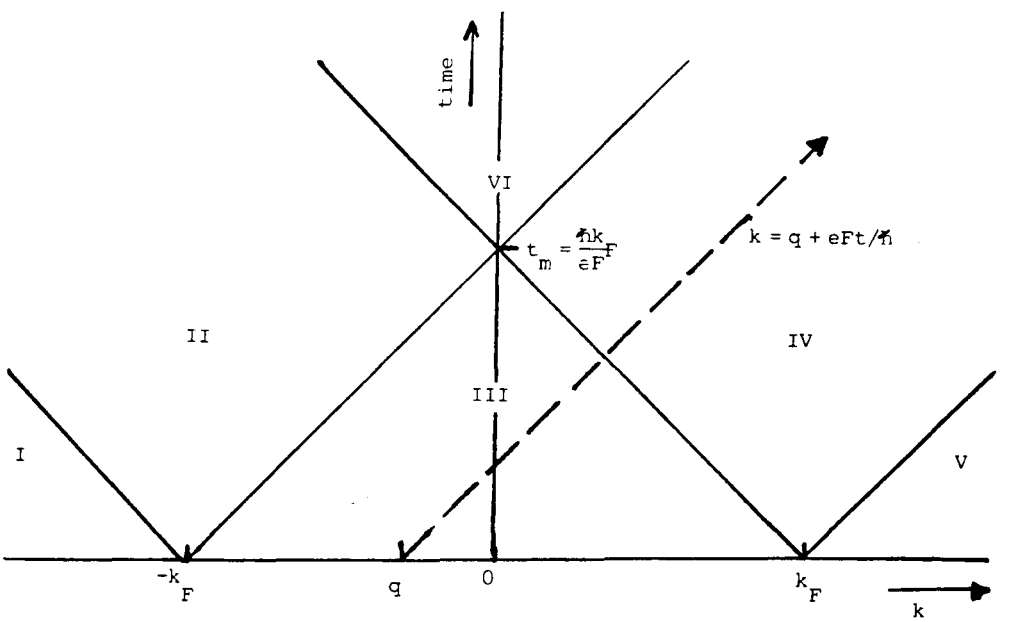

Fig.4.2.1. (k,t)-plane with six regions, all corresponding to different expressions for $g_k(t)$. The dotted curve indicates the path of integration to solve the inhomogeneous differential equation (4.2.7)

If we look more closely at $g_k(t)$, we see that $g_k(t)$ equals zero in the regions I, III, V of the (k,t)-plane (see fig. 4.2.1), which makes the integration trivial. In the other regions the integration is more complicated, but it is possible to express (4.2.11) in functions $J(\eta,\xi)$, defined by

$$J(\eta,\xi) = 1 - e^{-\xi} \int_0^{\eta} dt\, e^{-t}\, I_0[2\sqrt{\xi t}\,] , \qquad (4.2.12)$$

which are described by Luke [12]. Also tabular material of these integrals exists (see e.g. Brinkley and Brinkley [13]).

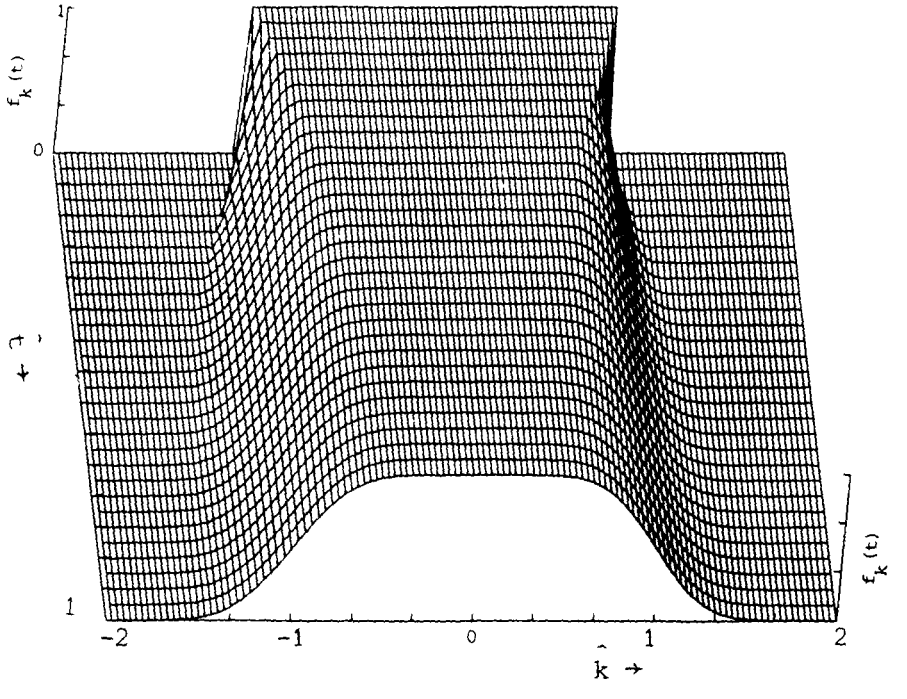

Fig.4.2.2. The probability distribution as function of the dimensionless wavenumber $\hat{k}$ and the dimensionless time $\hat{t}$ for $\hat{W}$=0.6 (for $\hat{k}$, $\hat{t}$ and $\hat{W}$ see text).

Using the dimensionless quantities, $\hat{t}=eFt/\hbar k_F$, $\hat{k}=k/k_F$ and $\hat{W}=\hbar k_F W/eF$, it is possible to rewrite the Boltzmann equation (4.1.16) in such a form that the initial three parameters (F, k_F and W) are replaced by only one parameter ($\hat{W}$). This implies that the shape of the function $f_k(t)$ does not change if we use other parameters F, k_F and W and leave $\hat{W}$ unchanged. The numerical integration of (4.2.11) is quite easy. As an example we calculated $f_k(t)$ in the case of $\hat{W}=0.6$, which is shown in fig. 4.2.2.

Both equation (4.2.11) and fig. 4.2.2 show that the probability distribution does not tend to a time-independent distribution. Nevertheless, it is possible to give an analytical proof that the current saturates after some time at the time-independent value $j_{sat}=e^2Fv_F/2\pi\hbar W$, where v_F is the Fermi velocity [6]. This fully resembles the situation in chapter 3, where it was also noticed that, although no stationarity was reached in any way, the current more or less saturated at a time-independent value.

For calculating the current j(t), the energy E(t) and the Boltzmann "entropy" S(t), we use

$$j(t) = \frac{e\hbar}{2\pi m}\int_{-\infty}^{\infty} dk\ k\ f_k(t), \qquad (4.2.13)$$

$$E(t) = \frac{\hbar^2 L}{4\pi m}\int_{-\infty}^{\infty} dk\ k^2\ f_k(t) \qquad (4.2.14)$$

and

$$S(t) = \frac{L}{2\pi}\int_{-\infty}^{\infty} dk\ f_k(t)\ \ln f_k(t). \qquad (4.3.15)$$

In fig. 4.2.3[a], 4.2.3[b] and 4.2.3[c] the current, the energy and the entropy are shown for the same case as mentioned above. The discussion of these results will be postponed until the next section.

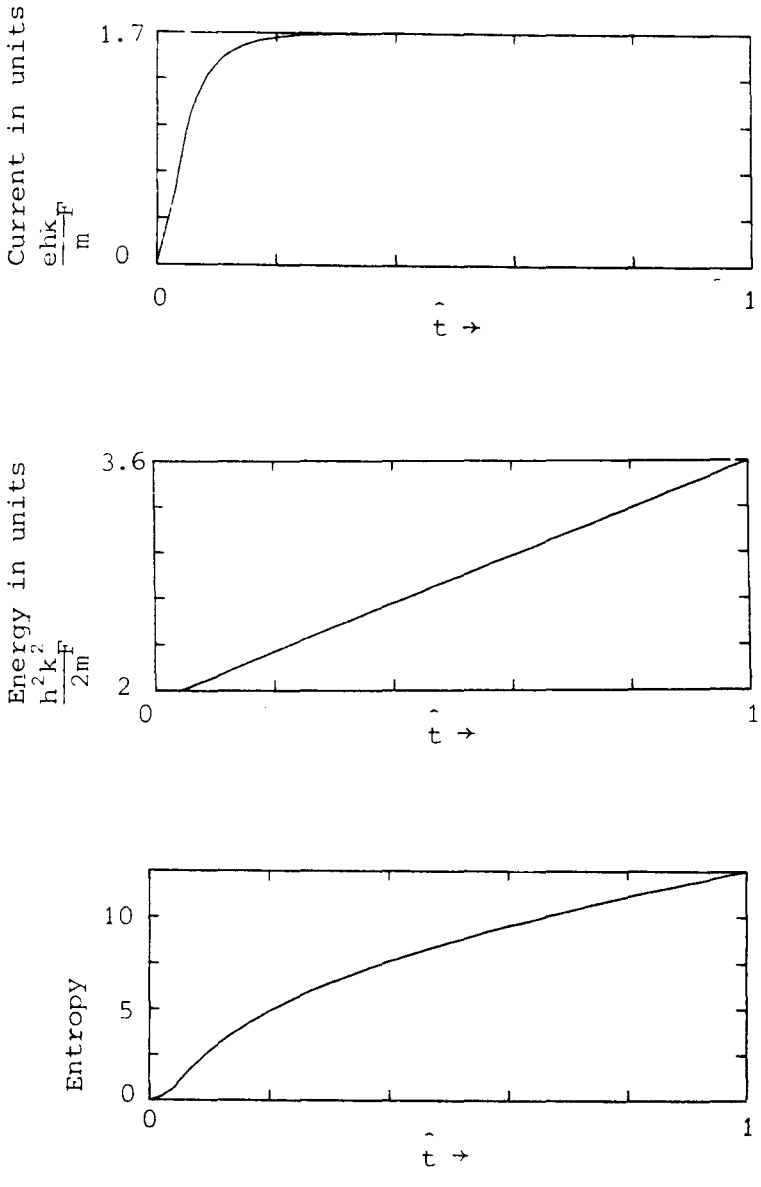

Fig.4.2.3[abc] The current, energy and entropy development as a function of the dimensionless time, $\hat{t}$. ($\hat{W}$=0.6)

4.3 Comparison with quantummechanical results.

We have now obtained two sets of results corresponding to the two different descriptions for our system. One is directly based on the Schrödinger equation, while the other is based on a Boltzmann equation. In principle the first method is exact, except for the two-dimensional perturbation theory, used to obtain the "stationary" states and energy bands. This latter approximation is required from a practical point of view rather than being a fundamental approximation. The description based on the Boltzmann equation is intrinsically an approximative one, since it is known beforehand, that precise details such as the (deterministic) fluctuations or eventual persistent correlations can impossibly be reproduced. In this section we will compare the numerical results obtained using the two above-mentioned methods. In this respect it is stated that most of the calculations in chapter 3 were for two electrons, initially occupying high-energy states (near the Fermi-energy) with opposite currents. In the Boltzmann approach on the other hand, we have always dealt with initial situations, in which all states with $-k_F < k < k_F$ were occupied, where k_F is the Fermi wave-number. However, it can be shown, using the linearity of the Boltzmann equation, that the solution for $f_k(t)$, with two electrons only, that is, one initially at k_F and the other at $-k_F$, has a simple relationship to the solution for $f_k(t)$ with all the $|k|$-points up to k_F occupied by say N electrons. This relationship is such that the respective currents and energies are just proportional to each other, i.e.

$$j^{(2)}(t) = \frac{2}{N} j^{(N)}(t) \quad ; \quad E^{(2)}(t) = \frac{2}{N} E^{(N)}(t) \qquad (4.3.1)$$

Unfortunately, this is not true for the entropy, simply because the entropy is not linear in $f_k(t)$. This is one of the reasons, why entropies poorly compare to each other as we will see below.

In fig. 4.3.1 we have drawn three different energy versus time curves. The solid curve, which is somewhat fluctuating, is the result calculated in chapter 3, with parameter values $\gamma_{n_F} = 0.0255$; $Z_{n_F} = 100$; $n_F = 200$. In the Boltzmann calculation we need values for the backscattering rate W (4.1.15) and the effective field strength F_{eff} (4.1.14). However, there is a small complication in that W and F_{eff} were considered in the Boltzmann approach to be level-independent, which is

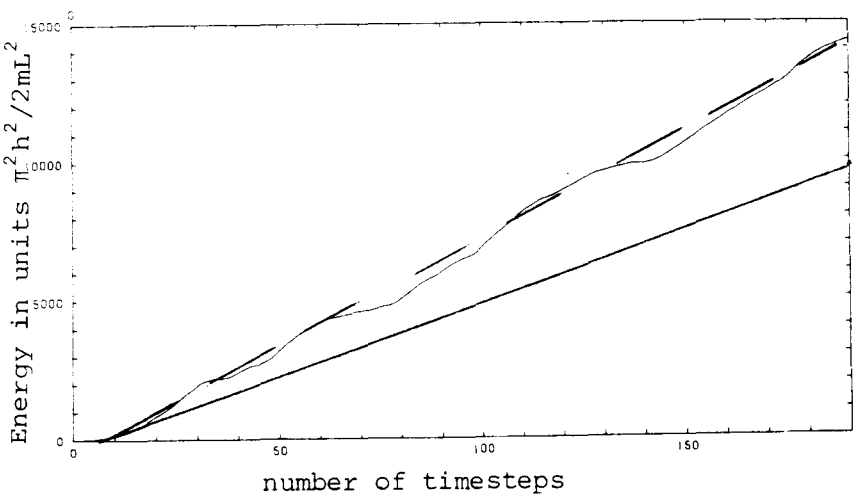

Fig. 4.3.1. The comparison of the energy curves corresponding to the two descriptions (see text). The somewhat fluctuating curve is the result obtained using the method of chapter 3, while the straight solid line is the result obtained using the Boltzmann approach (for the same parameters). The dotted line is obtained by fitting the backscattering rate in the Boltzmann approach.

an approximation.

When comparing Boltzmann results with those obtained in chapter 3, it seems reasonable to choose values for W and F_{eff} corresponding to their values in chapter 3 at the initally occupied levels. This leads to the straight solid line in fig. 4.3.1. The slope of this curve is seen to be smaller than the exact result by a factor of about 2/3. We do not really understand this large deviation. It seems as if the effective backscattering rate to be used in the Boltzmann approach is only 2/3 of the value which it is supposed to have at the Fermilevel (through (4.1.15)). One might even speak here of an "almost universal" effect, as can be seen from fig. 4.3.2. Apart from the straight line, this figure is taken from [9]. Each dot represents an average saturation current

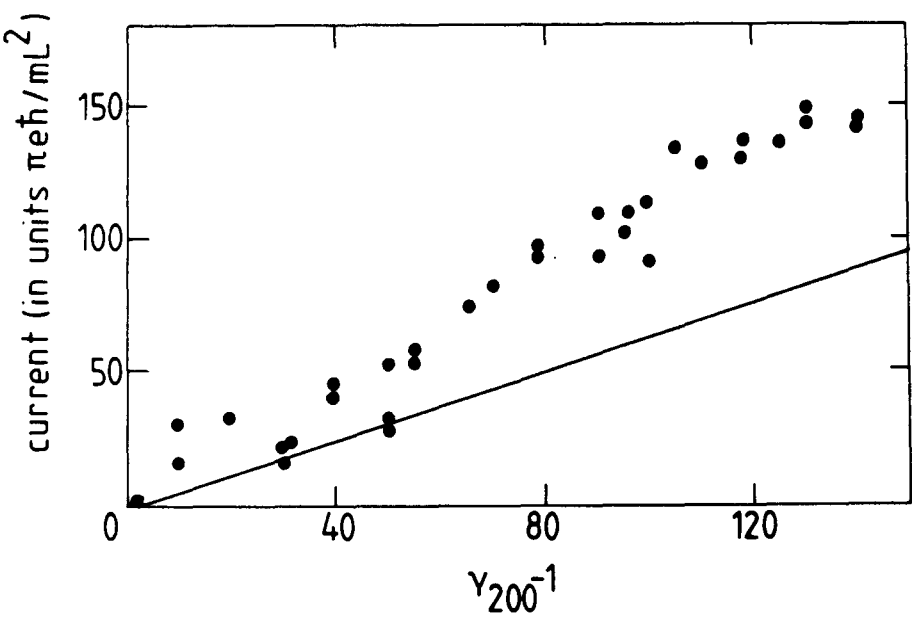

Fig.4.3.2. The dots indicate the saturation values obtained as a function of the field, which is proportional with γ_{n_F}. *The solid curve indicates the sateration values corresponding to the Boltzmann approach.*

level calculated at corresponding values of $\gamma_{n_F}^{-1}$ with n_F=200 and z_{n_F}=100. The straight line connects all corresponding results in the Boltzmann approach. In the majority of cases the true current is seen to be about 3/2 times as large as the Boltzmann prediction and this also suggests, that we are using an effective W, which is about 3/2 times too large.

We wish to emphasize that almost perfect reproduction (apart from fluctuations) of the energy curve can be obtained by optimal fitting of W. The best fit in this sense is the dotted curve in fig. 4.3.1, which has been obtained with a backscattering rate which is 0.677 times the old one.

The only possible explanation we can think of so far, is that, in spite of the quasi-randomness of phase angles, certain persistent correlations may exist which lead to a smaller backscattering rate, than expected. If such would be the case, our derivation of the Boltzmann equation in section 4.1 would still be suffering from a serious flaw. For the same parameters as in fig. 4.3.1, the respective current curves are given in fig. 4.3.3. These curves do not provide new information in

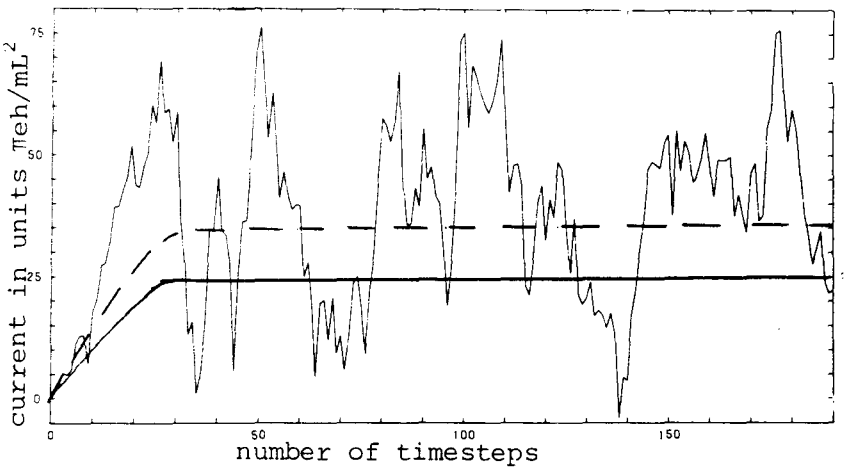

Fig.4.3.3. Currents as a function of time for the same cases as in fig.4.3.1.

view of the exact relation (3.2.1), which as a matter of fact is an exact relation between current and energy in the Boltzmann approach as well.

Let us now turn to the comparison of entropies. We observe remarkable differences between the two entropy curves in fig. 4.3.4 and 4.3.5. Not only their shapes are different, but also their magnitudes. All calculated "subjective" entropies (chapter 3) have the typical $\int$-shape, and, by construction are additive in the number of electrons. The Boltzmann approach entropy, however, exhibits no second kink and is not additive in the number of electrons. We wish to advocate here, that the "entropy" definitions used are not comparible to each other. In the Boltzmann theory, $f_k(t)$ is the probability in a many electron system for state k to be occupied by an electron. The $|c_n(t)|^2$ from chapter 2 on the other hand are probabilities for one given electron to occupy state (or band) n. Hence, we have to be careful when dealing with summations over electrons (chapter 3) and summations over states (chapter 4). For quantities, which linearly depend on both $f_k(t)$ and $|c_n(t)|^2$, such as current and energy, it is very well possible to compare results based on the two descriptions. This dependence is, however, non-linear for the entropy, which is the reason that similar expressions, that are different in the type of summations (i.e. over electrons or over states) lead to non-comparable results.

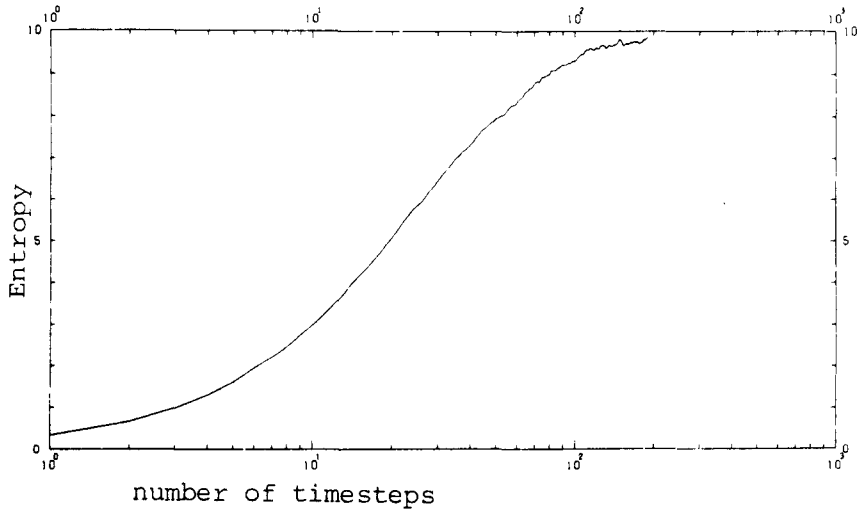

Fig.4.3.4. "Entropy", obtained using the method of chapter 3

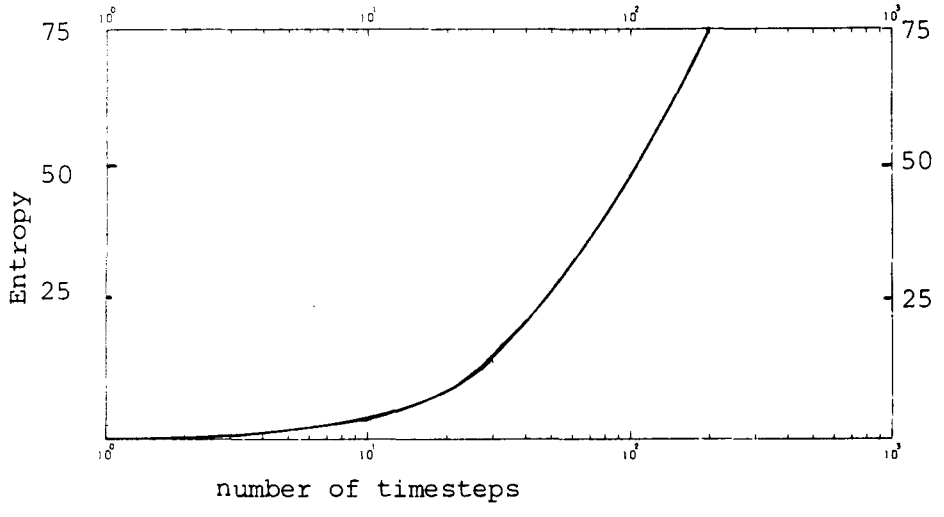

Fig.4.3.5. "Entropy" in the Boltzmann approach.

This can be illustrated by considering, e.g. the energy (2.4.14)

$$E(t) = \sum_{\text{electrons}} \left[\sum_{n} |c_n(t)|^2 \, \epsilon_n^{\alpha(t)} \right] \tag{4.3.2}$$

$$= \sum_{n} \left[\sum_{\text{electrons}} |c_n(t)|^2 \right] \epsilon_n^{\alpha(t)} \tag{4.3.3}$$

$$\Longleftrightarrow \quad \sum_{k} f_k(t) \, \frac{\hbar^2 k^2}{2m} \tag{4.3.4}$$

Hence, the two summation types are interchangeable. Consider now the "entropy" (3.3.2).

$$S(t) = \sum_{\text{electrons}} \left[\sum_{n} |c_n(t)|^2 \ln |c_n(t)|^2 \right] \tag{4.3.5}$$

$$\neq \sum_{n} \left[\sum_{\text{electrons}} |c_n(t)|^2 \ln \sum_{\text{electrons}} |c_n(t)|^2 \right] \tag{4.3.6}$$

$$\Longleftrightarrow \quad \sum_{k} f_k(t) \ln f_k(t). \tag{4.3.7}$$

Clearly (4.3.5) is different from (4.3.7). It might have been more adequate to start with (4.3.6) instead of with (4.3.5) as the definition of "entropy". In that case we expect to obtain results, which are better comparable to results based on (4.3.7). This expectation has not yet been verified.

References.

[1] R.Landauer, "Electrical resistance of disordered one-dimensional lattices", Phil.Mag. 21, 863-867, 1970.

[2] P.W.Anderson, D.J.Thoules, E.Abrahams and D.S.Fisher, "New method for a scaling theory of localization",Phys.Rev.B 22, 3519-3526, 1980.

[3] M.Buttiker, "Quantum oscillations in normal-metal loops",SQUID'85, Proceedings of the 3rd international conference on superconducting quantum interference devices, Berlin (West), edited by H.D.Hahlbohm and H.Lubbig, Walter de Gruyter, Berlin, New York, 1985.

[4] M.Buttiker, Y.Imry and R.Landauer, "Josephson behavior in small normal one-dimensional rings",Phys.Lett. 96A, 365-367, 1983.

[5] D.Lenstra and W.van Haeringen, "On the theory of DC conductivity at T=0K in a one-dimensional system of finite length: Calculation of the scattering rate in the case of weak disorder", J.Phys.C: Solid State Physics, 14, 5293-5303, 1981.

[6] D.Lenstra and W.van Haeringen, "DC conductance in a one-dimensional disordered system of finite lenght", J.Phys.C: Solid State Physics, 14, L819-L822, 1981.

[7] D.Lenstra and W.van Haeringen, "On the theory of DC conductance in a one-dimesional statically disordered system", Physica, 128B, 26-38, 1985.

[8] D.Lenstra, H.Ottevanger, W.van Haeringen and A.G.Tijhuis, "Metallic-like current response in small rings due to Zenertunneling", to be published in Phys.Scripta.

[9] D.Lenstra and W.van Haeringen, "Elastic scattering in a normal metal loop causing resistive behavior", Phys.Rev.lett. 57, 1623-1626, 1986.

[10] H.Ottevanger, "Elektrische geleiding in een een-dimensionale wanordelijke geleider", Masterthesis 1982-12, Delft University of Technology, Delft, the Netherlands, 1982.

[11] F.Oberhettinger, "Tabellen zur Fourier Transformationen", Springer Verlag, Berlin, 1957.

[12] Y.L.Luke, "Integrals of Besselfunctions", McGraw-Hill, Book Company, Inc, New York, 1962.

[13] S.R.Brinkely and P.F.Brinkley, "Table of the probability of hitting a circular target", Unpublished, See Math.Tables Aids to Comput., 2, 221, 1947.